https://doi.org/10.5194/egusphere-2026-4321
Preprint. Discussion started: 27 August 2026

Airborne and marine microplastics in the Northern Indian Ocean: decoupled pathways traced by black carbon

Piotr Markuszewski[1,2,3,4], Mikołaj Mazurkiewicz[1], Kinga Stawiarz[5], Małgorzata Śmiszek[5], Patrycja Jutrzenka-Trzebiatowska[6], Luca Ferrero[3], Krishnakant Budhavant[7,8], Mateusz Zawadzki[5], Anna Waleczek[9], Przemysław Makuch[1], Douglas Nilsson[2,4], Örjan Gustafsson[2,4], and Sophie L. Haslett[2,4]

[1]Institute of Oceanology, Polish Academy of Sciences, 81-712, Sopot, Poland
[2]Department of Environmental Science, Stockholm University, 10691, Stockholm, Sweden
[3]GEMMA and POLARIS Centre, Università degli Studi di Milano-Bicocca, Milano, Italy
[4]Bolin Centre for Climate Research, Stockholm University, 10691, Stockholm, Sweden
[5]Department of Physics of Electronic Phenomena, Institute of Physics and Applied Computer Science, Faculty of Applied Physics and Mathematics, Gdańsk University of Technology, ul. G. Narutowicza 11/12, 80-233 Gdańsk, Poland
[6]Department of Environmental Technology, Faculty of Chemistry, University of Gdańsk, 80-308 Gdańsk, Poland
[7]Maldives Climate Observatory-Hanimaadhoo (MCOH), Maldives Meteorological Services, H. Dh. Hanimaadhoo 02020, Maldives
[8]Divecha Centre for Climate Change, Indian Institute of Science, Bangalore 560012, India
[9]Faculty of Oceanography and Geography, University of Gdańsk, al. J. Piłsudskiego 46, Gdynia, 81–378, Poland

Correspondence to: Piotr Markuszewski (pmarkusz@iopan.pl)

Abstract. Microplastics (MPs) are increasingly detected in marine and atmospheric particulate matter, but their sources, transport, and air–sea exchange remain poorly constrained in remote marine regions. We investigated airborne microplastics (AMPs) and marine microplastics (MMPs) during a 1-month campaign at the Maldives Climate Observatory Hanimaadhoo and in adjacent coastal waters. Airborne particles were collected with a deposition box, and seawater was sampled at coastal sites. Particle morphology, size, and polymer composition were determined by optical microscopy and μ-Raman spectroscopy and evaluated alongside aerosol scattering and equivalent black carbon (eBC). AMP concentrations ranged from 0 to 10.3 MP m^{-3} (mean: 3.1 ± 2.8 MP m^{-3}). MMP concentrations ranged from 120 to 2656 MP m^{-3} (mean: 876 ± 804 MP m^{-3}), exceeding typical open-ocean values and indicating substantial local influence from inhabited islands and maritime activity. Significant differences in size distributions and pronounced compositional differences of AMPs and MMPs suggest weak coupling between the atmospheric and marine reservoirs. Low dry-season wind speeds probably suppressed wave breaking, bubble bursting, and sea-spray-mediated transfer from ocean to atmosphere. Instead, AMP variability coincided with polluted air-mass advection, elevated eBC, and enhanced aerosol scattering, indicating stronger control by regional atmospheric transport than by local marine emissions. These results show that remote island atmospheres are exposed to anthropogenic plastic aerosol transport and demonstrate the value of combining MP observations with established aerosol tracers to resolve plastic-particle pathways in marine environments.

https://doi.org/10.5194/egusphere-2026-4321
Preprint. Discussion started: 27 August 2026

1 Introduction

Microplastic (MP) contamination is now recognised as a widespread environmental problem affecting both the ocean and the atmosphere (Allen et al., 2022). The marine environment is considered a major reservoir of MPs. Still, these particles are also increasingly detected in air, where they behave as aerosol particles, can be transported over long distances, and may later be deposited back to the sea surface or land (Allen et al., 2019; Ferrero et al., 2022). This implies active exchange between the ocean and atmosphere and highlights the need to study both compartments together. Such interactions may be especially important in island regions of the Indian Ocean, where MP levels can be influenced by both local human activity and regional transport from densely populated and industrialised areas (Pattiaratchi et al., 2022).

MPs are generally defined as plastic particles smaller than 5 mm and typically larger than 100 nm (Kum et al., 2025). They are commonly divided into primary and secondary forms. Primary MPs are manufactured directly as small pellets or fibres, whereas secondary MPs originate from the degradation of larger plastic items through physical, chemical, or biological processes (Boucher and Friot, 2017). In the marine environment, MPs can affect a wide range of organisms and destabilise ecosystems, and global marine MP concentrations have increased substantially over recent decades (Auta et al., 2017). At the same time, airborne microplastics (AMPs) are emerging as an important concern in South Asia, where they are increasingly considered part of regional aerosol chemistry, raising questions about their sources, transport pathways, deposition, and long-term environmental and human health effects (Perera et al., 2022; Kannankai and Devipriya, 2024).

The Maldives is a particularly relevant setting in which to investigate these processes. The country consists of low-lying coral islands and is highly vulnerable to MP pollution because of its geographic exposure and limited waste-management capacity. Marine microplastics (MMPs) have already been documented across several Maldivian islands and atolls, including Vavvaru (Imhof et al., 2017), Naifaru (Patti et al., 2020), Faafu Atoll (Saliu et al., 2018), and Magoodhoo (Raguso et al., 2022). These studies point to a complex and interconnected pollution landscape, in which polymers such as polyethylene (PE) and polypropylene (PP) recur and may indicate shared source types and degradation pathways (Wang X. et al., 2020; Trainic et al., 2020). The ecological implications are substantial. MPs have been detected in reef-building corals, emphasising the vulnerability of one of the most biodiverse and sensitive ecosystems in the Indian Ocean, and reported impacts include tissue abrasion and the possible leaching of additives (Raguso et al., 2022; Isa et al., 2025). In contrast, much less attention has been paid to the role of airborne transport in redistributing plastic particles and influencing environmental concentrations, including those in the marine environment.

The regional anthropogenic context is equally important. In 2019, the Republic of Maldives was ranked as the fourth-largest per-capita waste producer globally (Stevens and Froman, 2019). This ranking is largely linked to rapid tourism growth and increasing urban waste generation (Rifa and Hossain, 2022). During the last decade, per-capita waste production increased by about 58 %, placing strong pressure on national waste-management infrastructure. A key symbol of this problem is Thilafushi, a lagoon converted into a landfill island in 1992, which now receives around 700 tons of waste daily from nearby islands (Kapmeier and Gonçalves, 2018; Kaza et al., 2018; Munshi et al., 2022). Open-air burning and unregulated

https://doi.org/10.5194/egusphere-2026-4321
Preprint. Discussion started: 27 August 2026

landfilling at Thilafushi are likely important regional sources of incomplete combustion products, including black carbon (BC) and potentially AMPs (Dasari et al., 2025). The open burning of mixed waste releases a complex mixture of pollutants, including fine and coarse particulate matter ($PM_{2.5}$ and PM_{10}), which may contain AMPs and BC, together with toxic gases and semi-volatile organic compounds such as carbon monoxide, volatile organic compounds, and polycyclic aromatic hydrocarbons (Budhavant et al., 2015; Kováts et al., 2022; Islam et al., 2022).

In the Maldives, the interaction between airborne and oceanic plastic pollution is of particular concern because of the country's geographic setting and strong dependence on marine resources (Royle et al., 2022). Air–sea exchange processes, including sea spray and windborne transport, are thought to facilitate the transfer of MPs between the ocean and atmosphere, even in remote environments (Ferrero et al., 2022). Deposition of AMPs into marine systems may increase toxicity in marine ecosystems (Ferrero et al., 2022), while the release of MMPs into the atmosphere through bubble-bursting processes may degrade air quality and increase risks to human health (Oehlschlägel et al., 2024). These source–sink relationships must therefore be constrained to understand how exchange processes influence both AMP and MMP populations.

Airborne transport is also directly relevant for human exposure. The size and aerodynamic diameter of MPs determine how deeply they can penetrate the respiratory system. Particles with aerodynamic diameters below 2.5 µm are considered respirable. They may reach the deep peripheral regions of the lungs, whereas particles between 2.5 and 100 µm are generally considered inhalable and deposit in the smaller and larger airways, respectively (Donaldson and Tran, 2002; Vasse and Melgert, 2024). Polymers such as PP, PE, and polyterephthalate (PET) have been reported among the predominant types detected in peripheral lung tissue (Donaldson and Tran, 2002; Vasse and Melgert, 2024).

AMPs also need to be considered within the broader atmospheric aerosol framework. Atmospheric aerosols in general, and absorbing aerosols in particular, play a key role in regional air quality and climate. In the Maldivian context, BC is especially relevant because it is emitted by incomplete combustion associated with open waste burning, diesel transport, biomass combustion, and residential energy use, all of which are plausible in island settings with limited waste-management capacity (Gustafsson et al., 2026; Bond et al., 2013; Ramanathan and Carmichael, 2008). In tropical and marine boundary layers, BC affects radiative balance, boundary-layer stability, and cloud microphysical processes, while also acting as an effective tracer of local and regional anthropogenic influence (Nair et al., 2023; Andreae and Rosenfeld, 2008; Ramanathan et al., 2001).

Recent studies suggest that AMPs may be co-emitted with absorbing aerosols from common sources such as waste burning, traffic-related abrasion, and urban activity, and may therefore frequently co-occur in polluted air masses (Dris et al., 2017; Brahney et al., 2021; Allen et al., 2022). MPs may also act as vectors for BC, trace metals, and organic pollutants, potentially modifying particle hygroscopicity, optical properties, and atmospheric residence times (Rochman et al., 2013; Wang Z. et al., 2020). Such interactions may increase human health risks by promoting the inhalation of chemically complex particle mixtures and by facilitating the long-range transport of anthropogenic pollution to remote marine and island environments (Zhang et al., 2020; Prata et al., 2020). However, the co-variability and coupling between AMPs and absorbing aerosols remain poorly constrained, particularly in remote island regions influenced by both marine aerosol production and combustion-derived particles.

https://doi.org/10.5194/egusphere-2026-4321
Preprint. Discussion started: 27 August 2026

To address these gaps, this study investigates MP contamination in both the atmospheric and marine environments around the Maldives using intensive one-month measurements conducted near the Hanimaadhoo research station. We test whether AMPs in the northern Indian Ocean are primarily linked to local oceanic emissions or to transported anthropogenic aerosol regimes. Specifically, the study aims to (1) quantify MMPs and AMPs and determine their physical properties and polymer composition, (2) assess whether air–sea interaction processes influence MP variability, and (3) evaluate potential interconnections between AMPs and absorbing aerosols such as BC as tracers of local anthropogenic pollution sources.

2 Measurements

2.1 Sampling site

Atmospheric sampling and the majority of water sampling were carried out at the Maldives Climate Observatory Hanimaadhoo (MCOH, 6.776ºN, 73.183ºE). The Republic of Maldives is an island nation located in the Indian Ocean. Hanimaadhoo, one of the larger islands, measures approximately 7 km long and 750 m wide. The climate observatory is located at the northern tip of the island. The present study forms part of a broader research project described by Stegelius et al. (2026).

MCOH is a well-established regional receptor site for studying atmospheric outflow from South Asia over the northern Indian Ocean. The site experiences minimal direct local, in-island anthropogenic emissions (Sheesley et al., 2012; Budhavant et al., 2018, 2023), making it particularly suitable for investigating aged aerosol transported from the Indian subcontinent and surrounding source regions, as well as for characterising regional background marine air masses. Previous studies at MCOH have documented strong seasonal contrasts in aerosol chemical composition, optical properties, black carbon, brown carbon, sulfate, and source-diagnostic tracers, reflecting the alternating influence of polluted continental outflow and cleaner marine air masses (Budhavant et al., 2018, 2020, 2023, 2024; Nair et al., 2023; Clarke et al., 2026).

During the winter period, from December to February, northeasterly winds dominate over the region (Ramana and Ramanathan, 2006; Nair et al., 2023; Budhavant et al., 2024). This circulation pattern facilitates the long-range transport of polluted and atmospherically processed air masses from the Indo-Gangetic Plain and other South Asian source regions towards the Maldives, including transport pathways over the Bay of Bengal and the Arabian Sea. The present January–February 2023 campaign was conducted during the established South Asian winter outflow regime, when MCOH is expected to be influenced by transported anthropogenic aerosol mixed with regional marine and island-scale contributions.

This winter regime contrasts with the summer monsoon, when south-westerly winds typically bring cleaner, moist marine air masses from the Southern Indian Ocean (Budhavant et al., 2018, 2020, 2023). This seasonal contrast makes MCOH a valuable receptor site for studying aerosol transport across the northern Indian Ocean. The present study, however, focuses specifically on the January–February winter outflow period.

https://doi.org/10.5194/egusphere-2026-4321
Preprint. Discussion started: 27 August 2026

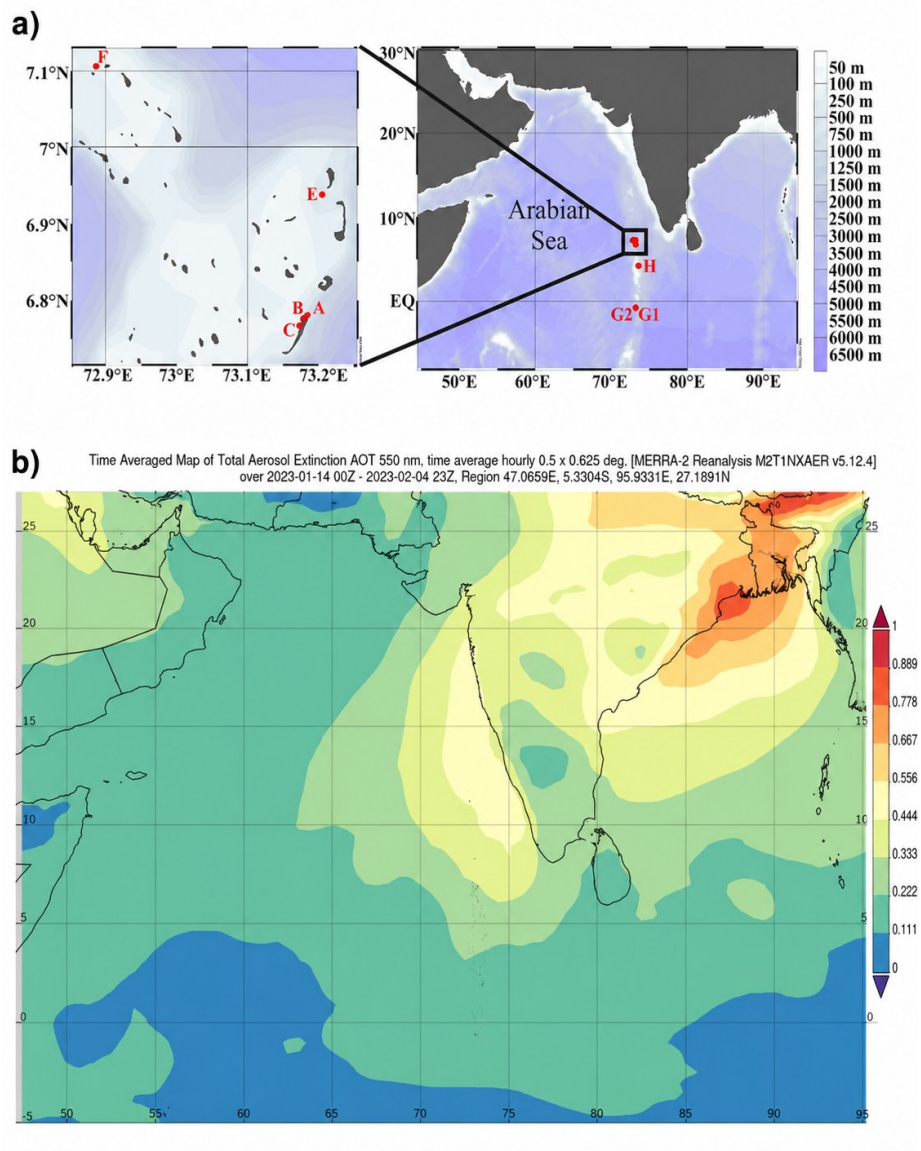

Figure 1. Study area, sampling locations, and regional aerosol conditions during the campaign in the northern Indian Ocean. (a) Location of the study area and sampling sites. The regional map shows the Arabian Sea and northern Indian Ocean, with bathymetry indicated by the colour scale in metres. The black box marks the Maldives archipelago. The detailed inset shows Hanimaadhoo Island and nearby islands, with coastal seawater sampling locations marked in red. A–C: Hanimaadhoo Island; E: Kelaa Island; F: Thuraakunu Island; G1–G2: Gan; H: Hulhumalé Island. Airborne microplastic measurements were conducted at the Maldives Climate Observatory Hanimaadhoo (MCOH). The maps were generated using Ocean Data View (ODV; Schlitzer, 2025). (b) Time-averaged total aerosol extinction aerosol optical thickness at 550 nm over the northern Indian Ocean for 14 January–4 February 2023, derived from MERRA-2 M2T1NXAER v5.12.4 (GMAO, 2015) and visualised using Giovanni (Acker and Leptoukh, 2007). The colour scale represents the regional aerosol loading and provides the atmospheric transport context for the microplastic observations.

https://doi.org/10.5194/egusphere-2026-4321
Preprint. Discussion started: 27 August 2026

2.2 Sample collection and laboratory procedures

2.2.1 Airborne sampling

In this study, Total Suspended MicroParticles (TSMP), including AMPs (González-Pleiter et al., 2021), were collected using a custom-built Deposition Box (Ferrero et al., 2018, 2022). This 50 × 50 × 20 cm^3 box, covered by a pitched roof to minimise environmental interference, integrates passive and active sampling features. Air is drawn at a flow rate of 1.5 m^3 h^{-1}, corresponding to approximately 30 air exchanges per hour. This results in a low internal flow speed (0.002 m s^{-1}), below ambient wind speeds. This creates conditions that favour dry deposition without particle stacking, thereby improving individual-particle isolation.

The Deposition Box was mounted on the tower's top at 15 meters above ground level. Glass microscope slides (26 × 76 mm^2) were used as substrates for the collection of TSMP. Prior to deployment, slides were cleaned with purified water and acetone, labelled, then stored in pre-cleaned, sealed aluminium containers. During sampling, they were secured on the stainless-steel grid inside the box and returned to the containers afterwards to minimise contamination.

In total, we collected 48 TSMP samples comprising 46 environmental samples and two laboratory blanks (samples 11 and 12) between 13th January and 4th February 2023. Sample exposure times ranged from 24 to 527 hours. This variation allowed AMP concentrations and deposition to be evaluated over different sampling periods. Once the collection was complete, the slides were immediately sealed in aluminium foil containers. The prepared samples were then transported to the laboratory for visual examination under a Leica M205C stereomicroscope.

2.2.2 Marine sampling

Seawater was collected using a 4 L metal bucket, which was flushed and cleaned with purified water before use. It was then poured through a 32 µm mesh stainless steel laboratory sieve. The material retained on the sieve was carefully transferred into pre-cleaned glass containers sealed with metal lids.

Water samples were collected at three different locations on Hanimaadhoo Island:

-the northern coast, at the closest possible distance from the measurement station (approximately 80 meters in a straight line, indicated as point A on Fig 1),

-the north-western coast (approximately 150 meters from the measurement station, indicated as point B on Fig 1),

-the central-western part of the island, adjacent to the local marina (indicated as point C on Fig 1).

In addition, to verify the spatial distribution of MMPs pollution, seawater samples were also collected on other islands in the Maldives archipelago: Kelaa, Thuraakunu, Gan, and Hulhumalé (marked with the letters E, F, G1, G2, and H in Fig. 1).

A total of 15 MMPs samples were collected. The range of filtered water was 27-80 dm^3.

The collected MMP samples were initially stored in 100 mL glass vials containing the original suspension. These bottles were placed in an oven and dried at 60 °C for 48 hours. Once dried, the samples were transported to the laboratory for further processing. At this stage, 30 % hydrogen peroxide (H_2O_2) was added to each bottle—ranging from 25 mL to 50 mL,

https://doi.org/10.5194/egusphere-2026-4321
Preprint. Discussion started: 27 August 2026

depending on the volume lost to evaporation—to oxidise organic matter. The samples were then subjected to a second drying cycle at 60 °C for an additional 48 hours, allowing further evaporation and decomposition of organic contaminants that otherwise could interfere with the analysis.

To isolate suspended materials, water samples were vacuum-filtered on glass fibre filters (Macherey-Nagel, grade MN 85/70, pore size 0.6 µm, diameter 55 mm), which were pre-heated at 450 °C for 4 hours to remove potential contaminants.

To facilitate visual detection of particles on the filters, each sample was divided in half and thoroughly mixed before being poured into the Büchner funnel. During the decantation process, some sediment grains adhered to the container walls. After filtration, each filter was placed into a glass Petri dish and dried in an oven at 60 °C. To prevent cross-contamination, the Büchner funnel was cleaned after every one to two filtrations.

Finally, the dried filters were examined under a Leica M205C stereomicroscope for visual identification and analysis of MP particles.

2.3 Optical identification

During microscopic analysis, strict precautions were taken to minimise the risk of AMP contamination. All procedures were conducted under a laboratory fume hood. Prior to examining each sample, the microscope and surrounding work surfaces were thoroughly cleaned with a paper towel moistened with water. To assess the potential for background contamination, three clean Petri dishes were exposed near the microscope for 24 hours. The number of fibres detected in these control dishes was 18, 20, and 29, respectively—equating to a contamination rate of less than one fibre per hour—thus considered negligible for the integrity of the results.

All samples were visually inspected under a Leica M205C stereomicroscope, and suspected MP particles were photographed at the highest achievable magnification (ranging from 7.8× to 160×) using an attached Leica DFC450 camera (5-megapixel resolution, 2560 × 1920 pixels, 3.4 × 3.4 µm pixel size). Each particle was then categorised by colour and shape, and its dimensions (length and width) were measured using the ImageJ software. The measurement of fibre length and width was conducted by means of the segmented line tool. Each fibre width was measured three to five times and averaged. For other particles, the polygon selection tool was used to outline them, enabling measurement of Feret diameters.

In the final phase of the study, selected marine and airborne samples were prepared for Raman spectroscopy to confirm the plastic nature of the particles and identify their polymer composition. During microscopic observation, the most distinctive items were marked with a pencil for marine samples and a 0.2 mm marker for airborne samples to clearly define the areas targeted for spectroscopic analysis.

Microscopy-derived particle data, including particle-size and morphology analyses, were processed and statistically analysed using R version 4.3.3 (R Core Team).

https://doi.org/10.5194/egusphere-2026-4321
Preprint. Discussion started: 27 August 2026

2.4 µ-Raman analysis

Raman spectroscopy was employed to identify the polymer type of suspected microplastic particles. Measurements were performed using a LabRam Aramis (Horiba Jobin Yvon) 460 mm spectrometer integrated with a confocal microscope. Two excitation sources were used: a diode-pumped solid-state laser at 532 nm (green) and a He-Ne laser at 632.8 nm (red). Spectra were recorded over a range of 400–3200 cm^{-1} with a spectral resolution of 2 cm^{-1}. For each measurement, 20 scans of 2 s each were collected. A diffraction grating with 600 grooves mm^{-1} and a confocal aperture (hole) of 200 µm was employed.

Particles were initially located under a 10× objective (numerical aperture 0.25), and individual spots were scanned using a 50× objective (numerical aperture 0.5), focusing the laser on a 1–2 µm area of the particle. Neutral density filters (optical density 0–2) were applied as needed to adjust the laser intensity. Spectral data were processed using the LabSpec software (Horiba) and compared with reference spectra from literature for polymer identification.

Successful spectral matching for airborne samples was constrained by several practical and material-specific factors, including (i) occasional particle loss during transport, (ii) fluorescence and/or advanced weathering that obscured diagnostic Raman bands, and (iii) the use of two excitation wavelengths (532 and 632 nm), which do not provide equally effective performance across all polymer classes and non-polymeric materials. For this reason, polymer identification was not based exclusively on spectral-library matching. Instead, assignments were made primarily through manual interpretation of diagnostic Raman bands in individual spectra. Where library comparison was possible and informative, only matches of at least 70 % were accepted; nevertheless, the majority of identifications relied on direct expert spectral interpretation rather than on automated matching alone. Polymer attribution was based on direct Raman confirmation whenever achievable and, where appropriate, complemented by a conservative morphology-guided assignment for visually comparable particles collected under the same sampling conditions—an approach considered justified only when a shared provenance is plausible (Perraki et al., 2024).

Morphology and colour were used as first-pass screening criteria to separate candidate plastics from organic and mineral matter (often brown and beige). Plastic fibres were typically characterised by uniform width and sharp, cut-like edges. A useful observation from this study is that fibres with a lint-like surface texture were frequently identified as PE by Raman spectroscopy. In contrast, cellulose fibres often displayed variable width, split/elongated edges, and a twisted-ribbon appearance. Fragments displayed either lint-like PE-type textures or smooth surfaces with adhered dust; films appeared as small foil-like pieces. Representative particles are shown in Appendix B (Figs. B1 and B2).

In some marine samples, Raman spectra were dominated by pigments, complicating polymer-level identification. In such cases, particles were treated as “plastic/unclassified” only when spectral features and morphology together supported a plastic origin.

https://doi.org/10.5194/egusphere-2026-4321
Preprint. Discussion started: 27 August 2026

2.5 Meteorological and Aerosol measurements

Wind speed and direction were measured using a Gill WindMaster Pro sonic anemometer mounted at the top of the tower, 18 m above ground level (a.g.l.). Relative humidity, air temperature, and rainfall were monitored using a Vaisala Weather Transmitter (WXT520), co-located at 18 m a.g.l., with a 3 min time resolution.

At MCOH, aerosol optical properties are monitored continuously. In the present study, aerosol absorption coefficients and instrument-estimated eBC (Petzold et al., 2013) were measured using a Magee Scientific AE33 aethalometer. The absorption data were corrected for filter multiple-scattering effects following Müller et al. (2014) and Ferrero et al. (2024). In this manuscript, eBC was derived from channel 6 (880 nm) of the AE33 and is used as a qualitative tracer of anthropogenic aerosol influence and regional atmospheric transport. No fossil-fuel versus biomass-burning source apportionment was applied to the aethalometer data, because such separation depends strongly on assumed source-specific absorption Ångström exponents and ideally requires independent validation, for example by radiocarbon-based ^{14}C source apportionment (e.g., Gustafsson et al., 2009).

Aerosol light scattering was measured using an integrating nephelometer (TSI Model 3563), which provided scattering coefficients at 450, 550, and 700 nm. Scattering data were corrected for truncation error following Müller et al. (2011). In the present study, the scattering coefficient at 550 nm was used for comparison with AMP observations.

Aerosol sampling was carried out through a PM_{10} inlet located at 15 m a.g.l. Ambient air was drawn through a vertical sampling line from the inlet to the aerosol instrumentation installed in the laboratory at the base of the tower. Further technical details on aerosol sampling at MCOH are provided by Corrigan et al. (2006) and Budhavant et al. (2018).

The aethalometer and nephelometer datasets were screened for instrumental artefacts and physically unrealistic values before averaging to the time base used for comparison with AMP samples. Periods affected by instrument instability, maintenance, invalid flow conditions, or obvious short-term spikes unrelated to ambient variability were removed. However, the data-cleaning procedure applied here was not identical to the most recent site-specific MCOH quality-control protocol used for long-term aerosol-climatology studies. Accordingly, the aerosol variables are interpreted primarily as campaign-scale contextual indicators and as tracers of co-variability with AMP concentrations, rather than as a standalone long-term aerosol dataset. This distinction is particularly relevant for absolute eBC and scattering values, whereas the directional contrasts discussed below are used mainly as supporting evidence for changes in air-mass influence.

Meteorological and aerosol data processing, including quality control, temporal averaging, and statistical analysis, was performed using MATLAB R2020b (version 9.9; The MathWorks, Inc., Natick, MA, USA).

3 Results and discussion

The field campaign was carried out during the dry phase of the winter monsoon, when north-easterly winds originating over the Indian subcontinent prevail (Budhavant et al., 2018, 2024; Ramachandran & Rupakheti, 2020). During this season, the arriving air masses often bear signatures of South Asian winter pollution as they traverse the Indian Ocean before reaching

https://doi.org/10.5194/egusphere-2026-4321
Preprint. Discussion started: 27 August 2026

the Maldives (Budhavant et al., 2018, 2023; Dasari et al., 2025). In addition to the monsoon-driven synoptic flow, local sea breezes and weak trade winds frequently develop around the islands. At the same time, regional ocean currents, influenced by monsoonal circulation, tend to remain relatively steady during the dry period. Although this season is generally characterised by scarce rainfall and stable temperatures—typical of the Maldives' equatorial setting, short-lived convective events and isolated thunderstorms may still occur, especially when local atmospheric conditions favour rapid vertical development. Below, detailed results are reported.

3.1 Microplastic concentrations

3.1.1 Airborne microplastics

AMPs accounted for approximately 9 % of TSMP. Among the 158 identified AMPs, fragments were slightly more abundant (86 particles; 54.4 %) than fibres (72 particles; 45.6 %). AMP concentrations ranged from 0 to 10.28 m^{-3}, with a mean of 3.06 ± 2.75 m^{-3} (mean ± standard deviation). Thus, AMPs were consistently present, but at low concentrations relative to the total suspended microparticle load, which was dominated by non-plastic material, notably cellulose. Detailed sampling results are provided in Appendix B (Tab. B2; Fig. B3).

Fig. 2 compares the mean AMP concentration observed here with previously published regional datasets. The MCOH mean exceeds those reported for the East Indian Ocean (Wang et al., 2020), Sri Lanka (Perera et al., 2022), and the Sundarbans (Ghosh et al., 2025) by nearly an order of magnitude or more, while remaining closest to the coastal Arabian Sea values reported by Kaushik et al. (2024). In this sense, the low fractional contribution of AMP to TSMP should not be interpreted as evidence of negligible atmospheric contamination, but rather as a consequence of the strong non-plastic background typical of coastal and marine air masses. This interpretation is consistent with Perera et al. (2022), who showed that only a relatively small fraction of visually selected outdoor airborne particles in Sri Lanka were ultimately confirmed as synthetic. In contrast, natural and semi-synthetic materials dominated the remainder.

At the same time, the absolute AMP concentrations observed here were substantial relative to the available literature from the Indian Ocean sector. They exceeded those reported for the northeast Arabian Sea by Kaushik et al. (2024), who measured mean concentrations of 1.30 ± 0.14 m^{-3} in 2016 and 1.46 ± 0.12 m^{-3} in 2020. They were markedly higher than the outdoor values reported from Sri Lanka by Perera et al. (2022) (0.00–0.23 m^{-3}). They were also above the open-ocean East Indian Ocean concentrations reported by Wang et al. (2020) (0.4 ± 0.6 items per 100 m^3) and the PM_{10} bound concentrations reported for the Sundarbans mangrove system by Ghosh et al. (2025) (10 ± 6 MPs per 100 m^3). Accordingly, although AMP represented only a modest fraction of TSMP, their abundance in air was comparatively elevated relative to several marine and coastal benchmarks from the wider Indian Ocean region.

https://doi.org/10.5194/egusphere-2026-4321
Preprint. Discussion started: 27 August 2026

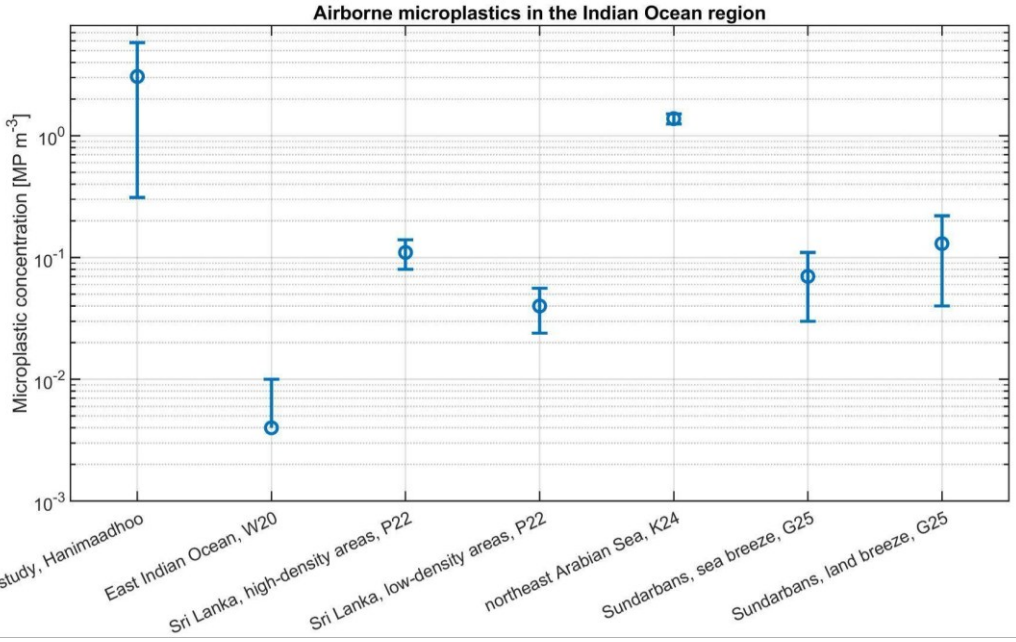

Figure 2. Regional variability in airborne microplastic (AMP) concentrations. The x-axis shows the sampling regions, along with abbreviations for the studies from which the concentration data were obtained: W20 – Wang et al. (2020), P22 – Perera et al. (2022), K24 – Kaushik et al. (2024), and G25 – Ghosh et al. (2025).

These comparisons should be interpreted cautiously because the available studies differ in sampling design, sample size fraction, air volume, filter material, and analytical workflow. Even so, a consistent regional pattern emerges: AMP levels are strongly shaped by source proximity, population density, and atmospheric setting. Very low concentrations in the East Indian Ocean (Wang et al., 2020) and in low-density coastal Sri Lankan sites (Perera et al., 2022) indicate strong dilution in marine air masses and limited local input, whereas higher concentrations in coastal Goa (Kaushik et al., 2024) and in the present study imply either stronger regional source influence, weaker dilution, or both.

The broader South Asian literature supports this interpretation. In Sri Lanka, the highest outdoor AMP abundances occurred near industrial and high-density areas, while no AMP were detected in some low-density coastal settings (Perera et al., 2022). Ghosh et al. (2025) likewise showed that, even at a remote mangrove island, atmospheric MP concentrations responded strongly to mesoscale meteorological conditions, with higher values during land-breeze and fog-influenced periods. Rao et al. (2025) further reported higher AMP concentrations in summer than in winter, attributing this to enhanced photodegradation and resuspension under warmer, drier, and windier conditions. Similar mechanisms may also operate in the Maldives, where high solar radiation, salt exposure, and episodic strong winds may promote fragmentation and intermittent aerosolisation despite the marine influence. By contrast, passive deposition studies in megacities report orders-of-magnitude higher loads (Tauhiduzzaman et al., 2025). However, such flux-based datasets are not directly comparable with active air concentrations expressed in m^{-3}.

https://doi.org/10.5194/egusphere-2026-4321
Preprint. Discussion started: 27 August 2026

Taken together, the available literature indicates that the Maldives AMP dataset does not represent a weak atmospheric signal. On the contrary, it documents a morphologically mixed, slightly fragment-dominated, PE/PP-rich AMP assemblage with concentrations that are high relative to several currently available Indian Ocean and South Asian marine and coastal studies (Wang et al., 2020; Perera et al., 2022; Kaushik et al., 2024; Ghosh et al., 2025; Rao et al., 2025). At the same time, the low AMP contribution to TSMP shows that these MPs were embedded within a much larger background of non-plastic atmospheric material. We therefore infer that AMPs were consistently present at regionally significant concentrations, but that their detectability in bulk aerosol terms was moderated by strong marine dilution and a large natural particulate background. This combination appears characteristic of a marine boundary layer influenced by both atmospheric transport and nearby coastal and maritime plastic sources.

3.1.2 Marine microplastics (MMP)

In seawater, the operational marine dataset comprised 663 particles. MMP number concentrations ranged from 120 to 2656 MP m^{-3}, with a mean of 876 ± 804 MP m^{-3}. Fibres accounted for 52 % of the identified particles, while fragments accounted for 48 %. Concentrations were calculated by dividing the number of MMPs identified in each sample by the volume of seawater filtered. Twelve highly elongated fibres measuring 5.18–9.13 mm were retained in the primary dataset according to the operational size criterion defined in Sect. 2. Applying the conventional upper size limit of 5 mm to all particle shapes reduced the mean concentration to 856 ± 794 MP m^{-3} but did not affect the overall interpretation of the results. Detailed site-specific sampling results are presented in Fig. B4 in Appendix B.

The highest concentrations occurred in sample 6 (2656 MP m^{-3}, collected at the MCOH station) and sample 7 (2060 MP m^{-3}, collected at Undhoali Beach near the marina), both sampled after a storm and both characterised by a high fragment fraction. This pattern is consistent with storm-related mechanisms that can increase observed MP abundance, including resuspension of nearshore material, redistribution of floating and neutrally buoyant particles, and mobilisation of coating fragments from vessels or infrastructure. A third high value was observed in sample 9 (2060 MP m^{-3}) near Thuraakunu Island, the most western site in this dataset. While this is less intuitive in a simple distance-from-source framework, it is consistent with the idea that concentrations at individual sites may be shaped by advection, local circulation, or episodic transport, rather than solely by immediate proximity to inhabited shorelines. The lowest concentrations were found in samples 12 and 14 (180 MP m^{-3} at the Gan and MCOH stations, respectively) and in sample 15 (120 MP m^{-3} at Hulhumalé Beach). Because these low values were observed at different coastal locations, no simple spatial gradient emerged. Filtered volume did not correlate with concentration, although smaller volumes typically increase counting uncertainty and can amplify sample-to-sample variability.

Fig. 3a further emphasises that the MMP signal was highly heterogeneous across sites, with no simple monotonic spatial trend. Instead, the distribution was characterised by sharp local maxima, particularly in the post-storm samples, superimposed on a background of substantially lower concentrations. This pattern supports the interpretation that MMP abundance around the Maldives is controlled by a combination of local inputs and short-term redistribution processes rather

https://doi.org/10.5194/egusphere-2026-4321
Preprint. Discussion started: 27 August 2026

than by distance from inhabited shorelines alone. In addition, at the Hanimaadhoo site, where repeated sampling under contrasting tidal conditions was available, a potential influence of tide height on MMP concentration was observed. Mean concentrations were substantially higher during high tide (1360 ± 882 MPs m^{-3}) than during low tide (409 ± 194 MPs m^{-3}). Although a similar pattern was not evident at the other sites, those locations were represented only by singular sampling events, which preclude an equivalent assessment of tidal effects. The Hanimaadhoo results suggest that local hydrodynamic conditions, including tidal stage, may influence nearshore MMP abundance through changes in water exchange, resuspension, and particle redistribution within the coastal zone.

For comparison with previous studies, Figure 3b presents all concentrations in a harmonised unit of items m^{-3}. On this basis, the mean concentration observed here (876 ± 804 MPs m^{-3}) is substantially higher than the values reported in the available Indian Ocean literature. The contrast is particularly strong with the two Maldivian studies of Saliu et al., which reported an average surface-water concentration of 0.26 particles m^{-3} in Faafu Atoll in 2018, with site values ranging from 0.02 to 0.48 particles m^{-3}, and in a subsequent survey reported mean values of 0.46 ± 0.15 items m^{-3} inside the atoll rim and 0.12 ± 0.09 items m^{-3} outside the reef.

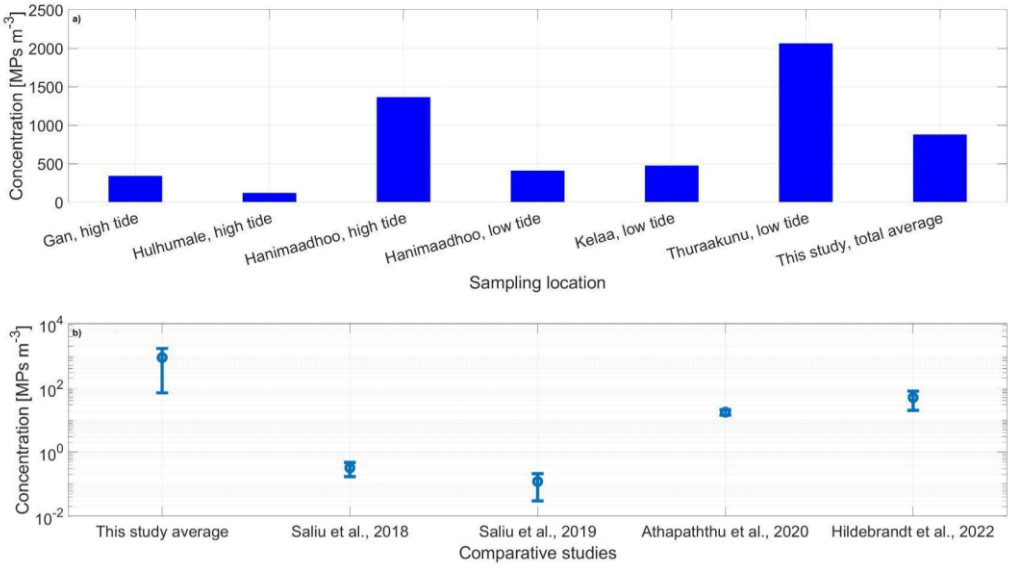

Figure 3. Spatial variability and regional comparison of marine microplastic (MMP) concentrations. (a) MMP concentrations were measured at the individual sampling sites in the Maldives study area. (b) Comparison of mean MMP concentrations (± standard deviation) from the present study with values reported in previous studies from the Indian Ocean region.

The present values are also clearly above those reported by Athapaththu et al. (2020) for southern coastal Sri Lanka, who found a mean microplastic density of 17.45 ± 3.35 items m^{-3} in surface waters, and by Hildebrandt et al. (2022) for the tropical Indian Ocean, who reported 8–132 particles/fibers m^{-3} with a mean of 50 ± 30 particles/fibers m^{-3} for the 20–300 µm fraction, while the >300 µm fraction averaged only 0.1 ± 0.4 MP m^{-3}.

https://doi.org/10.5194/egusphere-2026-4321
Preprint. Discussion started: 27 August 2026

Accordingly, Figure 3b shows that the concentrations measured in the present study are higher than those reported in the comparison datasets by roughly one to two orders of magnitude relative to Athapaththu et al. (2020) and Hildebrandt et al. (2022), and by several orders of magnitude relative to the Maldivian seawater values of Saliu et al. (2018, 2019).

This difference likely reflects not only environmental forcing but also methodological contrasts among studies. A particularly important factor in the present work is that seawater was directly poured through a 32 µm stainless-steel laboratory sieve, which likely enhanced the recovery of the smallest particles and increased the total number of items. This is important because many Indian Ocean seawater studies rely on manta or neuston nets with substantially larger mesh sizes, typically 150–500 µm, and such approaches inevitably underrepresent the fine end of the microplastic size spectrum.

Even with this methodological divergence, the comparison strongly suggests that the present Maldives dataset does not represent a low-level open-ocean background. Rather, it indicates a markedly elevated nearshore MMP burden, consistent with strong local anthropogenic inputs associated with inhabited islands, coastal infrastructure, tourism, and maritime activity, as well as episodic storm-driven and tidal redistribution processes. The potential influence of the Indian Ocean "garbage patch" was also considered (Connan et al., 2021). Although this accumulation zone contains high levels of plastic macro-debris, studies with overlapping sampling areas do not necessarily report elevated MP concentrations in surface waters and therefore do not support it as the dominant explanation for the high abundances observed here. Instead, the site-specific peaks in Figure 3a and the broader contrast shown in Figure 3b indicate that MMP concentrations around the Maldives are more strongly influenced by local anthropogenic inputs and short-term hydrodynamic forcing than by large-scale oceanic accumulation zones.

Taken together, these results indicate that MMP concentrations around the Maldives are highly variable in space and time and are shaped by a combination of local source strength, storm-related remobilisation, and, at least at Hanimaadhoo, a probable tidal control on nearshore particle abundance. In this context, the present dataset appears to reflect a coastal-island system in which MP concentrations are driven primarily by local anthropogenic influence and episodic redistribution processes. The comparison with previous Indian Ocean studies is further complicated by substantial differences in sampling resolution, particularly regarding the lower size limit retained.

3.2 Microplastic dimensions and shape

Quantifying the dimensions of MP particles is central to their classification and interpretation, including whether particles fall within the formal MPs size definition and how efficiently they may be transported and deposited in the atmosphere or aquatic environment (Arthur et al., 2009; European Commission, 2011; Zeng, 2023). Non-fibrous particles were classified as MPs when their maximum dimension was ≤5 mm. Owing to their highly elongated geometry, fibres were retained up to a length of 15 mm when their length-to-width ratio exceeded 3. Twelve marine fibres measuring 5.18–9.13 mm and one airborne fibre measuring 6.92 mm met this criterion. A sensitivity analysis was additionally performed using the conventional 5 mm upper size limit for all particle shapes.

https://doi.org/10.5194/egusphere-2026-4321
Preprint. Discussion started: 27 August 2026

The AMP length distribution was strongly right-skewed (Fig. 4a), with an overall mean of 546 µm and a median of 297 µm. This pooled distribution reflects the contrasting dimensions of the two principal morphologies rather than a numerical dominance of short fibres. Fragments, which accounted for 54.4 % of the identified AMPs, were substantially shorter, with a mean length of 251 µm and a median of 216 µm. Fibres were less numerous but considerably longer, with a mean length of 899 µm and a median of 526 µm, and therefore contributed disproportionately to the upper tail of the distribution. The concentration of observations in the sub-millimetre range may be consistent with fragmentation and weathering at the source, followed by morphology-dependent aerodynamic selection during atmospheric transport. However, particle dimensions alone cannot distinguish conclusively between these processes or identify a specific source.

The overall mean AMP length observed in the present study was close to the mean particle sizes of 525–538 µm reported by Kaushik et al. (2024) and somewhat lower than the mean of approximately 643 µm reported by Wang et al. (2020) for the East Indian Ocean. For fibres specifically, the present median of 526 µm was close to the value of 551 µm reported by Perera et al. (2022), whereas the mean fibre length of 899 µm was higher than that reported by Perera et al. (2022; 769 µm) but lower than the fibre means of approximately 1086–1125 µm reported by Kaushik et al. (2024). Consequently, the present dataset does not provide evidence for a general enrichment in short fibres. Instead, its relatively low overall median primarily reflects the substantial contribution of comparatively short fragments. These comparisons should nevertheless be interpreted cautiously because the studies differed in sampling design, lower detection limits, and particle-identification procedures.

The AMP width distribution showed two clearly separated groups (Fig. 4c), but this structure was associated predominantly with particle morphology. Fibres were generally narrow, with a mean width of 15.9 µm and a median of 15.0 µm, whereas fragments were substantially broader, with a mean width of 132.8 µm and a median of 110.2 µm. Of the 73 particles narrower than 32 µm, 70 were fibres, while 83 of the 85 particles wider than 32 µm were fragments. Thus, the broad-width group should not be interpreted primarily as a separate population of thick technical fibres or rope-derived filaments. Instead, the width distribution largely reflects the coexistence of narrow, elongated fibres and broader fragments.

This morphological separation may nevertheless have implications for atmospheric transport. Narrow fibres can potentially remain suspended efficiently because of their elongated geometry and relatively low settling velocity, whereas broader fragments would generally be expected to undergo more rapid gravitational removal. Such behaviour also depends on particle density, orientation, surface roughness, and atmospheric turbulence. The observed width structure therefore supports a morphology-dependent difference in transport efficiency, but it does not by itself demonstrate that the broader particles originated locally or that the narrower fibres were transported over longer distances.

The marine fraction was nearly balanced, with fibres accounting for 52 % of MMPs and fragments for 48 %. This near-even partition indicates that seawater contained both elongated and non-elongated particles in comparable proportions. In the broader Indian Ocean context, that balance is plausible. The recent Indian Ocean review shows that fibres and fragments are the two dominant MP forms in seawater across the basin, with fibres contributing about 53 % and fragments about 34 % in non-trawl sampling studies, and slightly more balanced proportions in trawl-based datasets. Athapaththu et al. (2020) reported that filaments were the dominant morphotype in southern coastal Sri Lanka, while Li et al. (2022) also identified

https://doi.org/10.5194/egusphere-2026-4321
Preprint. Discussion started: 27 August 2026

fibres as the dominant shape in the southern Indian Ocean. Thus, the present MMP morphology is consistent with regional evidence, but with a higher fragment share than the most fibre-dominated coastal datasets.

MMP size distributions were strongly right-skewed and heterogeneous (Figs. 4b and 4d). Much of the observed size structure was associated with particle morphology. Fibres were substantially longer, with a mean and median length of 1284 and 923 µm, respectively, and narrower, with a mean and median width of 16 and 12 µm. Fragments were shorter (mean: 119 µm; median: 90 µm) and broader (mean: 59 µm; median: 50 µm).

The broad MMP size range remains consistent with observations from the Indian Ocean, although direct comparison is complicated by differences in sampling and analytical methods. Athapaththu et al. (2020) found that more than 45 % of MPs in southern Sri Lankan coastal waters were <1 mm, with more than 25 % in the 400–600 µm range. Li et al. (2022) reported that the most common size class in the southern Indian Ocean was 500–1000 µm (38.5 %), followed by 100–500 µm (28.85 %). They reported a size range of 108–4703 µm and an average particle size of 1060 ± 991 µm, overlapping with much of the fibre-size range observed in the present study.

By contrast, Hildebrandt et al. (2022) reported a much finer distribution in the tropical Indian Ocean: 75 % of the detected MPs were in the 20–50 µm range, 21 % were in the 50–100 µm range, and 96 % were <100 µm. This difference probably reflects both methodological and environmental factors. Hildebrandt et al. (2022) sampled subsurface water at 6 m depth and targeted very small particles using highly sensitive fractionated filtration, whereas the present study focused on nearshore waters and retained a broader particle-size spectrum. Direct comparison is therefore meaningful only when differences in sampling depth, mesh size, and analytical size limits are considered.

The MMP width distribution likewise primarily reflected morphological differences rather than two independently fitted particle populations. The narrow fraction was dominated by fibres, whereas fragments and coating-derived particles contributed mainly to the broader fraction. This separation may be related to differences in particle production, hydrodynamic behaviour, and environmental retention. Nevertheless, particle dimensions alone cannot demonstrate particle origin or distinguish conclusively between local fragmentation, transport, and remobilisation processes.

Overall, AMP and MMP size distributions primarily reflected differences between fibrous and fragment-like particles. Fibres generally formed the narrower and longer fraction, whereas fragments formed the broader and shorter fraction. The two environmental compartments nevertheless differed significantly in their particle-size distributions, indicating that the atmospheric and marine assemblages were shaped by different combinations of particle morphology, transport, and

https://doi.org/10.5194/egusphere-2026-4321
Preprint. Discussion started: 27 August 2026

environmental retention.

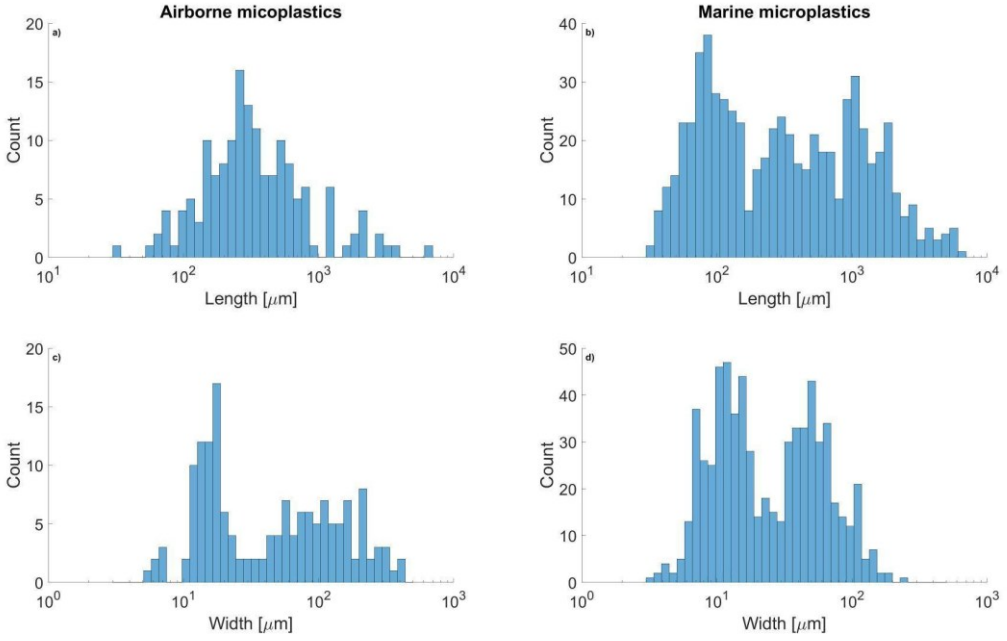

Figure 4. Size distributions of airborne and marine microplastics (AMP and MMP) shown on logarithmic scales. The upper panels present (a) AMP length distribution and (b) MMP lengths. The lower panels present (c) AMP width distribution and (d) MMP width distribution.

3.3 Polymer composition and morphological properties

Figure 5a, b shows the relative contribution of polymer types identified in AMPs and MMPs, respectively. In the airborne fraction, PE was the dominant polymer (51 % of identified AMP), followed by PP (28 %), PET (5 %), and polyamide (PA, 1 %); 15 % of AMPs could not be assigned because no sufficiently robust match was obtained in the μ-Raman analysis. This pattern broadly overlaps with South Asian atmospheric datasets, indicating that PE, PP, and PET are recurrent airborne polymers, although their relative proportions vary substantially across environments. For example, Ghosh et al. (2025) identified only four polymers in the Sundarbans atmosphere (PET, PE, PP, and polystyrene), with PP and PE dominating especially during sea-breeze conditions, whereas Rao et al. (2025) reported a Delhi NCR aerosol signal dominated by PET (41 %) and PE (27 %). In contrast, Perera et al. (2022) found that outdoor AMPs in Sri Lanka were dominated by PET (48 %), followed by polyester (PES, 34 %), PA (14 %), and acrylic (4 %), while Kaushik et al. (2024) reported a chemically distinct Arabian Sea aerosol signature dominated by polyvinyl chloride and polymethyl methacrylate, followed by PES and other polymers. Thus, the present airborne assemblage is not simply identical to previously reported coastal or island datasets, but is best described as a polyolefin-rich atmospheric mixture, with PE and PP clearly more prominent than in the Sri Lankan or Delhi datasets and far more prominent than in the Goa aerosol record (Kaushik et al. 2024).

https://doi.org/10.5194/egusphere-2026-4321
Preprint. Discussion started: 27 August 2026

The pie charts in Fig. 5 do not by themselves identify the source, and it would be too strong to state that the observed polymers are definitively packaging- or fishing-derived. It can be said that the AMPs' polymer pattern is consistent with that of common secondary consumers and of maritime plastics. That inference is based on the known uses of these polymers and on comparison with the literature, not on the pie charts alone. PE and PP are widely used in packaging, household items, ropes, and fishing-related materials; PET is common in textiles, bottles, films, and packaging; and PA is frequently associated with textiles, ropes, and nets. In this sense, the present AMPs spectrum is consistent with a mixture of widely used low-density consumer plastics and maritime materials, but it is not diagnostic of a single source class.

This distinction is important, particularly because the Sri Lankan study interpreted its PET-rich airborne signal mainly in terms of textile sources, while Ghosh et al. (2025) linked PP- and PE-rich atmospheric particles to a mixture of fishing-net material, packaging waste, and marine or coastal reservoirs under contrasting breeze regimes. The present results suggest a mixed marine-coastal-atmospheric source pool, but they do not allow direct apportionment among packaging, fisheries, and other uses.

A further point that deserves explicit discussion is that the observed contrast between atmosphere and seawater may reflect not only different source regimes, but also different particle properties. In particular, PE and PP are low-density polyolefins and are more likely to remain at or near the sea surface, where they are more available for wind-driven resuspension and sea-spray-mediated exchange. By contrast, PET and PA are denser polymers, so they are more likely to remain suspended in the water column, sink, or be removed from the atmosphere more efficiently when present as compact fragments. Thus, the lower PET proportion in AMP and the higher PET proportion in MMPs may indeed reflect, at least in part, differential environmental partitioning and source differences. This does not prove that the observed air–water contrast is controlled primarily by density, but it does mean that the contrast should not be interpreted as purely source-driven. Rather, the observed distribution likely reflects the combined effects of source regime, polymer density, buoyancy, particle size, and shape-dependent deposition behaviour.

Figure 5b shows that the marine fraction was compositionally distinct from the airborne one. For the MMP analysed by µ-Raman, the material composition was dominated by paint particles containing dye (32.4 %) and PET (24.4 %), unclassified plastic particles (18.4 %), and polycarbonate (13.9 %). Smaller contributions were made by polypropylene (5.6 %), polyamide (4.5 %), and polyethylene (0.8 %). Several particles were categorised as unclassified plastic because dye or pigment signatures precluded confident polymer assignment, even though they were clearly plastic-like. The high contribution of paint-related particles is consistent with observations in the tropical Indian Ocean, where Hildebrandt et al. (2022) reported that acrylates/polyurethane/varnish-like particles accounted for 49 % of detected polymer clusters and PET for 26 %, with much smaller contributions from PP (8 %) and PE (4 %). In this respect, the present seawater dataset does not resemble a simple PE/PP-dominated open-water assemblage. Instead, it shows a strong enrichment in coating-like particles and PET, in good agreement with the Hildebrandt dataset.

A striking feature of the present MMPs dataset was the unusually high occurrence of pink fragments, which were brittle, intensely coloured, and visually consistent with paint chips. Raman spectra suggested the presence of a dye, likely

https://doi.org/10.5194/egusphere-2026-4321
Preprint. Discussion started: 27 August 2026

rhodamine. Their predominance in post-storm samples supports the interpretation of localised emissions and mobilisation associated with storm-driven abrasion, as well as the release of material from marine coatings on vessels, harbour infrastructure, or coastal installations. The data support a substantial paint/coating contribution, but they do not identify a single unique source. A cautious interpretation is that coating-derived particles formed an important local source category in seawater and became particularly prominent after storm forcing.

The polymer distribution in the present seawater samples also differs from several broader reports from the Indian Ocean, in which PE and PP are described as among the dominant marine polymers. For example, a recent review of Indian Ocean monitoring data concluded that the main polymer types reported across the basin are PE, PP, and PS (Zhou et al., 2025), while another recent Indian Ocean study identified rayon, PE, PP, and PET as predominant materials (Wang et al., 2025). Against that background, the strong prominence of paint-related particles and PET in the present MMPs appears distinctive, though not anomalous in light of Hildebrandt et al. (2022). The most likely explanation is that broad basin-scale syntheses integrate many settings dominated by diffuse consumer plastic inputs, whereas the present samples capture a more localised island-maritime signal, shaped by proximity to infrastructure and storm-enhanced mechanical release.

The observed contrast between airborne and marine particle classes may also have implications for hazard, although this point should be treated cautiously. Based on Fig. 5 alone, toxicity cannot be ranked reliably by polymer type, because hazard depends not only on the base polymer, but also on particle size, morphology, weathering state, additive content, pigment load, and sorbed contaminants (Prata et al., 2024). Even so, the dominant particle classes identified here are unlikely to be equivalent. The marine fraction, enriched in paint/coating particles, deserves particular attention because such materials are chemically complex and may contain pigments, dyes, stabilisers, and other additives (Turner, 2021). In contrast, elongated airborne particles can remain suspended and contribute to inhalation exposure (Eberhard et al., 2024). Accordingly, the present results do not support the view that all identified polymers have the same environmental or health relevance; rather, they suggest that risk likely varies among particle classes, even though that variability cannot be resolved quantitatively from the present dataset alone.

On the whole, the polymer data suggest a system in which the airborne fraction is dominated by common polyolefins, likely reflecting a mixed secondary-consumer and maritime-plastic signal, whereas the marine fraction is enriched in paint/coating-related particles and PET, indicating a stronger imprint of local maritime sources. However, this apparent contrast should not be attributed solely to source differences. Polymer-specific properties such as density, buoyancy, morphology, and deposition behaviour are also likely to influence whether particles are preferentially retained in air or seawater. At first glance, the behaviour of MPs appears partly decoupled between the atmosphere and the ocean, but this decoupling most likely reflects a combination of source regime and particle properties rather than a single factor. Further data supporting this interpretation are presented in the next section.

https://doi.org/10.5194/egusphere-2026-4321
Preprint. Discussion started: 27 August 2026

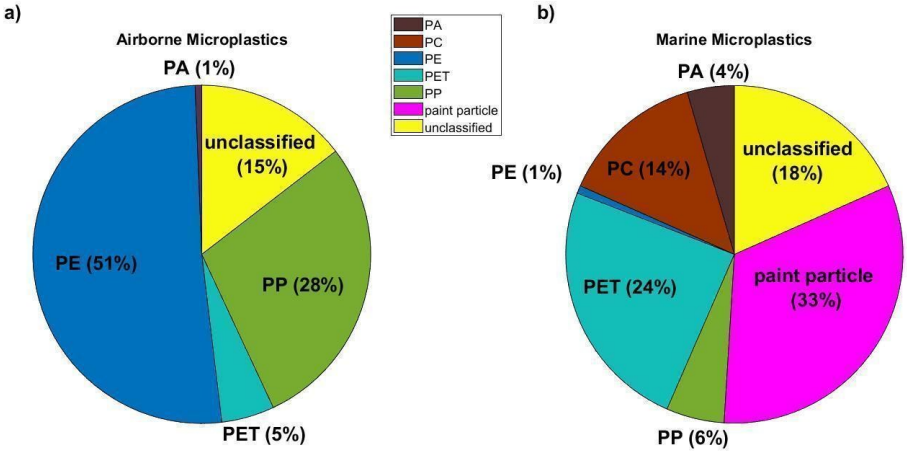

Figure 5. Relative abundance of polymer types among all identified microplastics: a) airborne sampling polymer composition; b) marine sampling polymer composition.

3.4 Air and marine microplastics comparison at MCOH site

In the preceding sections, microplastic properties were analysed using the full dataset, encompassing all sampling locations across the study area. In the following section, the analysis is restricted to a subset of samples collected in the immediate vicinity of the MCOH station. This approach ensures spatial consistency between airborne and marine datasets and enables a more direct comparison of their properties under comparable environmental conditions.

The dimensional distributions of AMP and MMP are compared in Fig. 6. For this analysis, the MMP data include only samples collected in the vicinity of the airborne measurement station to ensure spatial consistency between the two datasets (Sampling sites A and B in Fig. 1).

https://doi.org/10.5194/egusphere-2026-4321
Preprint. Discussion started: 27 August 2026

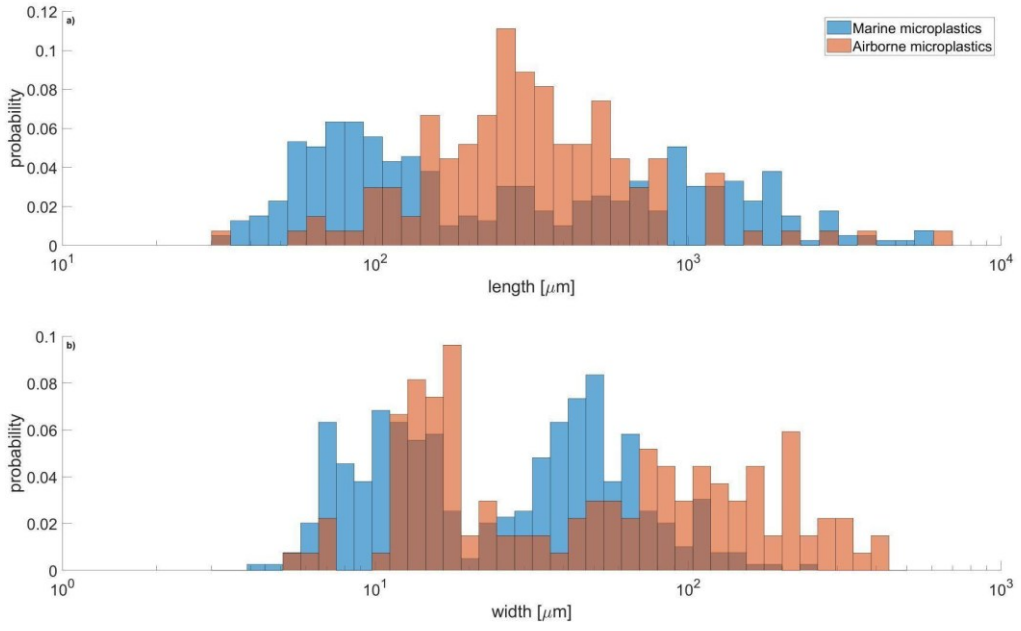

Figure 6. Probability distributions of particle dimensions for airborne and marine microplastics. Histograms compare airborne microplastics (orange) and marine microplastics (blue) measured during the campaign. Panel (a) shows the length distribution of microplastic particles, while panel (b) shows the width distribution.

The length and width distributions of AMP and MMP differed substantially (Fig. 6). Within the MCOH subset used for this comparison, marine fibres had a median length of 930 µm and a median width of 11 µm, whereas marine fragments had a median length of 86 µm and a median width of 49 µm. Airborne fibres had corresponding median dimensions of 526 and 15 µm, while airborne fragments had median dimensions of 216 and 110 µm. Thus, the broad peaks visible in the distributions largely reflect the coexistence of fibrous and fragment-like morphologies rather than independently fitted statistical modes.

To assess whether the length and width distributions of MMP and AMP differ statistically, we applied Kolmogorov–Smirnov tests. The results indicate that the two MP properties resulted with highly significant differences (p-values $< 10^{-8}$).

These differences can be interpreted in the context of environmental processes governing MP transport. Wind speed is a key control mechanism linking air-sea exchange, as it controls wave breaking, bubble entrainment, and sea spray aerosol production—all key pathways for MP transfer from the ocean to the atmosphere. Numerous studies have documented that sea spray aerosol fluxes increase sharply with wind speed due to enhanced turbulence and bubble-bursting activity (Lewis and Schwartz, 2004; O'Dowd & de Leeuw, 2007). Under high-wind conditions, such processes could entrain MP into the marine boundary layer (Allen et al., 2020; Ferrero et al., 2022). Conversely, during the dry season in the Maldives, mean wind speeds are very low, resulting in weak surface turbulence and minimal sea–air coupling.

These calm conditions strongly suppress the mechanisms responsible for upward MP transport, thereby reducing the likelihood that oceanic plastics contribute appreciably to the AMP population. Low winds likewise limit the atmospheric

https://doi.org/10.5194/egusphere-2026-4321
Preprint. Discussion started: 27 August 2026

deposition of airborne particles onto the sea surface. Together, these factors indicate that the AMP sampled during our campaign likely originates from sources or processes decoupled from the immediate marine environment, rather than from local ocean-to-atmosphere exchange. Thus, the observed statistical differences between AMP and MMP size distributions reflect not only the inherent variability in MP sources and fragmentation processes but also the Maldives' environmental regime during the dry season. The weak wind forcing helps to explain why the two reservoirs appear largely disconnected, highlighting the importance of seasonal meteorological conditions when interpreting MP exchange across the air–sea interface.

To sum up, the statistical differences between AMP and MMP size distributions suggest that the two reservoirs were only weakly connected during the study period, highlighting the importance of seasonal meteorological conditions in regulating microplastic exchange across the air-sea interface.

3.5 Pattern of air mass advection

Meteorological conditions during the campaign were generally calm, with an average wind speed of 2.34 ± 1.48 m s^{-1} and occasional stronger episodes, including a maximum gust of 12.48 m s^{-1} recorded on 23 January at 22:36 UTC. Precipitation was limited, although short periods of intense rainfall occurred, with the highest rate reaching 16.8 mm h^{-1} recorded on 24 January at 00:00 UTC. Aerosol loading exhibited substantial variability: the mean aerosol scattering coefficient at 550 nm was 47.6 ± 20.4 Mm^{-1}, peaking at 115.5 Mm^{-1} at 04:00 UTC on 23 January. The eBC concentrations were also elevated, averaging 1.75 ± 0.71 μg m^{-3}, with a maximum value of 3.7 μg m^{-3} observed at 7:00 UTC on 30 January 2023.

During the measurement campaign, the prevailing wind direction oscillated between the north-northwest and east sectors. These shifts in air mass origin were accompanied by differences in both TSMP and AMP characteristics. To account for the influence of air mass advection on AMP properties, we categorised the samples into two groups: those associated with predominantly northerly flow (wind directions between 305° and 14°) and those associated with easterly flow (wind directions between 47° and 96°). This distinction enables a more explicit examination of how changes in advected air masses affect the observed AMP concentrations. All AMP sample results are presented in Fig. 7 in a polar plot.

https://doi.org/10.5194/egusphere-2026-4321
Preprint. Discussion started: 27 August 2026

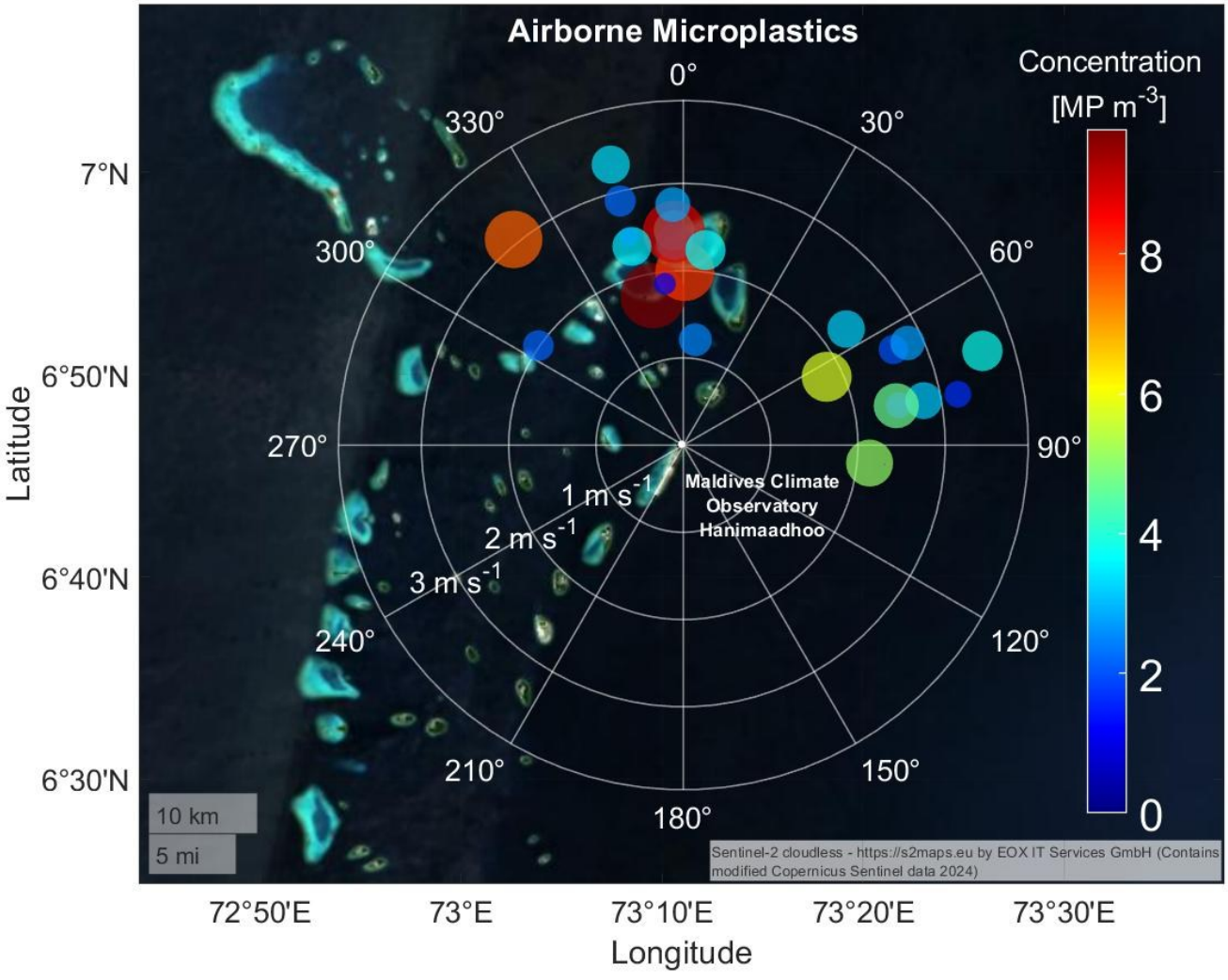

Figure 7. The concentrations of airborne microplastics (AMP) measured using the Deposition Box are presented as a polar plot. Angles from 0° to 359° represent the prevailing wind direction for each measurement series, and radial distance from the center of the plot represents wind speed in m s^{-1}. The size and colour of each circle represent concentration in MP m^{-3}.

Figure 8 illustrates the key differences between northerly and easterly wind patterns, showing the mean values and corresponding 95 % confidence intervals for both TSMP and AMP concentrations. For TSMP, the concentrations were higher under northerly flow (36.0 ± 32.0 m^{-3}) than under easterly flow (23.0 ± 14.1 m^{-3}). A similar pattern was observed for AMP: concentrations were higher during northerly advection (3.8 ± 3.2 m^{-3}) than during easterly advection (2.0 ± 2.0 m^{-3}). There was a large and overlapping standard deviation in both cases, for both TSMP and AMP, indicating that a large spread of concentrations were observed under both wind patterns. Under the northerly wind regime, the observed AMP concentrations were bimodal, with this wind direction producing both the highest and the lowest values. For the TSMP, the

https://doi.org/10.5194/egusphere-2026-4321
Preprint. Discussion started: 27 August 2026

difference in concentration between the two regimes is not statistically significant (Kolmogorov-Smirnov test p-value = 0.51), while the AMP comparison shows a statistically significant difference (p-value = 10^{-3}).

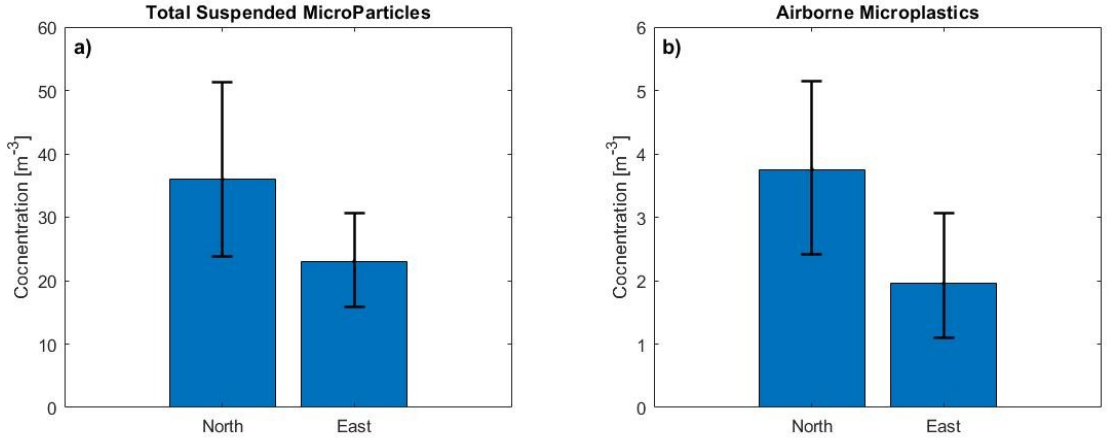

Figure 8. Comparison between north and east air mass advection for mean concentration values of total suspended microparticles (left panel) and airborne microplastics (right panel), with 95 % confidence intervals indicated as error bars.

Figure 9 compares the aspect ratios of TSMP and AMP under northerly and easterly advection and the calculated aerodynamic diameters of AMPs. TSMP exhibited a higher mean aspect ratio under northerly advection (32.4 ± 28.5) than under easterly advection (24.5 ± 28.0). In contrast, AMPs had a lower mean aspect ratio under northerly flow (8.3 ± 16.8) than under easterly flow (15.8 ± 32.1). Because AMPs represented only 9 % of TSMP, these opposing patterns suggest that the elevated TSMP aspect ratio under northerly advection was primarily driven by elongated non-plastic particles, potentially including cellulose or other natural fibres. Within the AMP subset, however, particles associated with easterly advection were more elongated on average. AMPs also exhibited a larger mean aerodynamic diameter under easterly than northerly advection (4.1 ± 3.8 and 2.9 ± 1.8 mm, respectively), although this difference was not statistically significant (p=0.5). The aerodynamic-diameter contrast should therefore be interpreted as a tendency rather than evidence of a distinct transport regime.

In addition to concentrations and aerodynamic diameter, differences among polymer compositions were examined. PE was the dominant polymer type in air masses from both directions, and also the percentages of PP and PET remained comparable; however, there was a visible dominance of PE from the east wind direction (62 %) compared with the north wind (46 %).

https://doi.org/10.5194/egusphere-2026-4321
Preprint. Discussion started: 27 August 2026

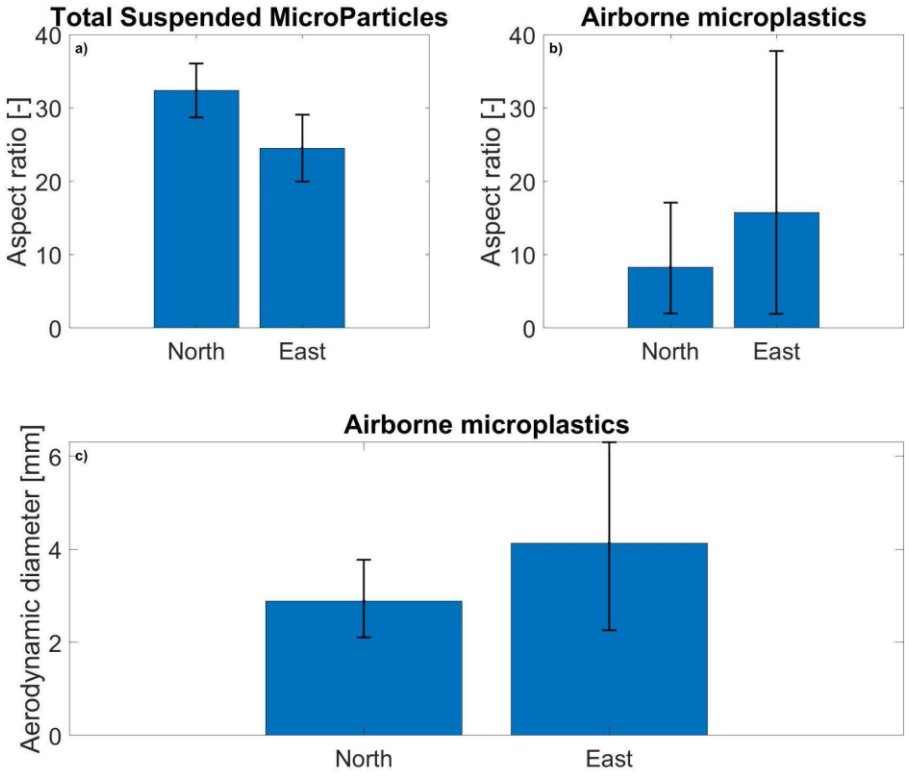

Figure 9. Mean physical properties comparison of measured airborne particles. Upper panels present aspect ratios (length/width) of total suspended matter and airborne microplastics. The lower panel presents the aerodynamic diameter of airborne microplastics. Error bars represent 95 % confidence intervals.

Taken together, these results indicate that air-mass origin influenced AMP abundance and properties, with northerly flow associated with higher concentrations and easterly flow characterised by relatively longer, aerodynamically larger plastic particles.

3.6 Equivalent black carbon and aerosol scattering as anthropogenic tracers to MP

During the campaign, the mean eBC concentration was 1.75 ± 0.71 μg m^{-3}, and the mean aerosol scattering coefficient at 550 nm was 47.6 ± 20.4 Mm^{-1}. These values indicate that the study period was characterised by appreciable aerosol loading, consistent with the dry-season South Asian outflow regime previously documented at MCOH. Earlier work has shown that MCOH is an important receptor site for polluted South Asian air masses, including transport from the Indo-Gangetic Plain and surrounding source regions. For example, Budhavant et al. (2024) reported substantial processing of black and brown carbon during transport over the Indian Ocean, while Nair et al. (2023) showed that BC at MCOH is sensitive to changes in South Asian emissions and decreased markedly during the COVID-19-related emission reductions. In this context, the eBC

https://doi.org/10.5194/egusphere-2026-4321
Preprint. Discussion started: 27 August 2026

levels observed during the present January-February 2023 campaign are consistent with a polluted wintertime receptor regime rather than with a clean marine background.

The comparison in Figure 10 further illustrates the relationship between air-mass advection, eBC, and aerosol scattering. Both variables show higher values under northerly advection than under easterly advection, consistent with the AMP patterns discussed above. Mean eBC concentrations were 1.94 ± 0.86 μg m^{-3} for northerly flow and 1.41 ± 0.65 μg m^{-3} for easterly flow. Aerosol scattering showed a similar directional contrast, with higher values under northerly advection (51.0 ± 22.4 Mm^{-1}) than under easterly advection (36.1 ± 12.8 Mm^{-1}). The corresponding violin plots, together with the confidence intervals, indicate that the northerly sector was associated with a systematically stronger aerosol signal overall.

This co-variability provides important context for interpreting AMP abundance. BC is a well-established tracer of anthropogenic combustion influence and regional transport, whereas aerosol scattering reflects the total concentration of light-interacting particles in the atmosphere. Here, an increase in both of these parameters is associated with elevated AMP concentrations, suggesting that AMP abundance responded coherently to the broader aerosol burden and to the degree of anthropogenic influence.

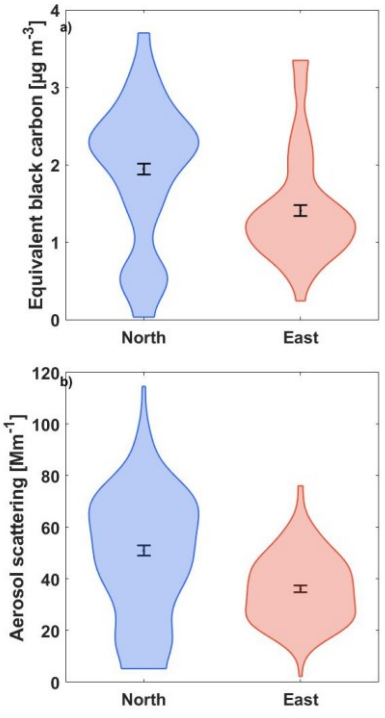

Figure 10. Violin-plot comparison of aerosol properties under contrasting air-mass advection regimes. Panel (a) shows equivalent black carbon (eBC) concentrations, and panel (b) shows the aerosol scattering coefficient at 550 nm, each separated into northerly and easterly advection patterns. The violin shapes represent the data distribution for each regime, central markers indicate mean values, and error bars denote the corresponding 95 % confidence intervals. Together, the plots illustrate the enhancement of both BC and aerosol scattering under northerly advection relative to easterly flow.

https://doi.org/10.5194/egusphere-2026-4321
Preprint. Discussion started: 27 August 2026

At the same time, the two tracers should not be interpreted in the same way. BC is more directly linked to combustion-derived emissions and is therefore useful as an indicator of anthropogenic input, whereas aerosol scattering integrates a wider range of particle types, including both anthropogenic aerosol and natural components such as sea spray and mineral dust. For this reason, scattering should be regarded as a broad indicator of total aerosol loading rather than as a specific tracer of microplastic sources. Nevertheless, its enhancement together with eBC and AMP under northerly advection strengthens the interpretation that these air masses carried a stronger near-surface aerosol signal overall.

The higher abundance of eBC, aerosol scattering and AMP concentration during the northerly wind regime, coupled with the large particle size and therefore likely short atmospheric lifetime of the observed AMPs, may at first suggest an aerosol mass influenced by emissions from adjacent islands to the north of Hanimaadhoo. However, concurrent observations of organic aerosol properties using an Aerosol Mass Spectrometer (Stegelius et al., 2026) did not reveal a signature of local emissions influencing the site from the north. In contrast, the chemical characteristics of aerosol observed during this campaign were broadly consistent, regardless of air mass history. Fresh, local emissions contributed less than 5% to organic aerosol mass, and did not increase with northerly wind. The remainder demonstrated features characteristic of aged, transported aerosol. The aerosol population observed during this campaign therefore represents a largely secondary, regionally mixed, sulfate-rich and highly processed haze (Stegelius et al., 2026). Previous studies support this interpretation carried out at this site, which indicate that aerosol observed at MCOH during the winter has undergone extensive regional mixing and atmospheric processing during long-range transportation. The most prominent identified source region at this time of year is the Indian sub-continent (e.g., Budhavant et al., 2018, 2024; Spencer et al., 2008).

The co-variation of AMPs with both the eBC and aerosol scattering signal therefore indicates that a long-distance source for these particles may be plausible. Although the current understanding of airborne transportation processes for AMPs is still limited and existing studies are few, there is increasing evidence that AMP transportation across vast distances may be possible (Enyoh et al., 2019). For example, Chen et al. (2023) observed AMPs of length 1004.8 ± 823.5 µm and diameter 49.8 ± 39.5 µm in the remote Southern Ocean and Antarctica, which had been transported thousands of kilometres. Similarly, van der Does et al. (2018) reported that giant dust particles (>75 µm) can be transported surprisingly vast distances, suggesting that the same may be possible for large AMPs.

A second plausible explanation, supported by the larger abundance of AMPs in the northerly wind regime, is that local emissions of AMPs from local islands may be superimposed on top of an already large aerosol background. Thus, while the majority of observed aerosol is dominated by long-distance transport and photochemical ageing processes, the AMPs may represent the dominant factor in a more local source.

4 Conclusions

This study provides a coupled assessment of MMPs and airborne AMPs in the northern Indian Ocean, based on intensive one-month observations conducted at the Maldives Climate Observatory Hanimaadhoo and in the surrounding coastal

https://doi.org/10.5194/egusphere-2026-4321
Preprint. Discussion started: 27 August 2026

waters. By integrating MP characterisation with aerosol optical and chemical measurements, it constrains the physical properties, sources, and transport pathways of MPs in a remote island environment.

First, the concentration, size, colour, and polymer composition of both AMP and MMP were quantified. MMPs occurred at concentrations substantially higher than those typically reported for open-ocean regions, indicating a strong influence of local anthropogenic activity associated with inhabited islands, coastal infrastructure, and maritime operations. Both compartments showed broadly balanced fibre-to-fragment proportions, although fibres were slightly more abundant in the marine dataset, whereas fragments were slightly more abundant among AMPs. Polymer compositions were broadly consistent with regional studies, although the high contribution of paint- or coating-related fragments points to a distinct localised source likely linked to ship-related materials.

Second, comparison of AMPs and MMPs revealed pronounced and statistically significant differences in size distributions, indicating weak coupling between the two reservoirs during the observation period. The low wind speeds characteristic of the dry season likely suppressed air–sea exchange processes such as wave breaking and bubble bursting, thereby limiting ocean-to-atmosphere transfer of MPs. Under these conditions, the observed AMP population appears largely decoupled from the local MMP pool and instead more strongly influenced by terrestrial and coastal emission sources.

Third, a clear co-variability between AMPs, eBC, and aerosol scattering was identified. Elevated AMP concentrations coincided with enhanced eBC and increased aerosol scattering under northerly advection, showing that AMPs varied coherently with established anthropogenic aerosol tracers. This relationship indicates that BC-like tracers can help constrain AMP transport regimes, especially in environments where local emissions and regional advection overlap. At the same time, the combined evidence suggests that both long-range transport and superimposed local emissions may contribute to the observed AMP signal, and a more definitive source apportionment will require further targeted analysis.

Taken together, these results show that MPs should be integrated into atmospheric transport frameworks rather than treated only as a marine pollution problem. They also demonstrate that remote marine atmospheres are not necessarily isolated from anthropogenic plastic aerosol transport, even in apparently ocean-dominated settings such as the Maldives. More broadly, the combined analysis of AMPs, MMPs, air–sea interaction processes, and aerosol tracers provides a robust framework for disentangling local emissions, regional transport, and exchange processes in island environments, although more detailed source apportionment will be needed to fully resolve their relative contributions. Integrating MP observations with established aerosol measurements will therefore be essential for improving our understanding of how plastic particles are transported through the atmosphere and redistributed across remote marine regions.

Appendix A: Acronyms

AMP – airborne microplastic

BC – black carbon

eBC – equivalent black carbon

https://doi.org/10.5194/egusphere-2026-4321
Preprint. Discussion started: 27 August 2026

MCOH - Maldives Climate Observatory Hanimaadhoo

MP – microplastic

MMP – marine microplastics

PA – polyamide

PC – polycarbonate

PE – polyethylene

PES – polyester

PET – polyethylene terephthalate

PM_{10} – Particulate Matter 10

$PM_{2.5}$ – Particulate Matter 2.5

PP – polypropylene

PS – polystyrene

TSMP – Total suspended microparticles

https://doi.org/10.5194/egusphere-2026-4321
Preprint. Discussion started: 27 August 2026

Appendix B: Supporting tables and figures

Table B1. Basic statistical characteristics of aerosol and airborne microplastic sampling and results of the Kolmogorov-Smirnov testing between air mass advection patterns.

	median		mean		Standard deviation		Min-max		1st-3rd quantiles		K-S test	
Advection type	N	E	N	E	N	E	N	E	N	E	h	p
TSMP, m^{-3}	26.3	25.2	36.0	23.0	32.0	14.1	9.5-133.6	4.6-46.74	15.0-38.3	9.7-30.0	0	0.51
AMPs, m^{-3}	3.2	1.7	3.8	2.0	3.2	2.0	0-9.8	0-7.6	0.6-6.1	0.5-2.6	**1**	10^{-3}
eBC, µg m^{-3}	2.15	1.27	1.94	1.41	0.86	0.65	0-3.74	0.22-3.38	1.48-2.51	0.98-1.60	**1**	10^{-43}
Scattering, Mm^{-1}	53.0	35.5	51.0	36.1	22.4	12.8	4.2-115.5	1.5-76.7	35.1-68.4	25.3-45.0	**1**	10^{-31}
TSMP, Aspect ratio, -	29.0	16.44	32.40	24.53	28.51	27.98	1.20-181.05	1.08-157.41	4.97-49.91	1.75-43.74	**1**	10^{-4}
AMPs, Aspect ratio, -	1.61	1.90	8.32	15.75	16.79	32.05	1.29-60.66	1.62-104.36	1.43-2.75	1.70-18.91	**1**	10^{-2}
AMPs, aerodynamic diameter, mm	2.09	2.32	2.89	4.13	1.83	3.81	0.77-6.08	0.88-12.79	1.36-4.38	1.82-6.76	0	0.5

https://doi.org/10.5194/egusphere-2026-4321
Preprint. Discussion started: 27 August 2026

Table B2. Deposition-box sampling periods and exposure times.

AMP sample no.	start year-month-day time	Stop, year-month-day time	exposure time, days
1	23-01-13 7:18	23-01-14 8:15	1.04
2	23-01-13 7:18	23-01-15 9:20	2.08
3	23-01-13 7:18	23-01-17 6:00	3.95
4	23-01-13 7:18	23-01-17 6:00	3.95
5	23-01-13 7:18	23-02-04 7:00	21.99
6	23-01-13 7:18	23-02-04 7:00	21.99
7	23-01-13 7:18	23-01-19 6:45	5.98
8	23-01-13 7:18	23-01-19 6:45	5.98
9	23-01-13 7:18	23-01-27 7:14	14.00
10	23-01-13 7:18	23-01-27 7:14	14.00
11	23-01-13 7:40	23-02-04 7:00	21.97
12	23-01-13 7:40	23-02-04 7:00	21.97
13	23-01-14 8:15	23-01-19 6:45	4.94
14	23-01-15 9:20	23-01-17 6:00	1.86
15	23-01-17 6:00	23-01-19 6:45	2.03
16	23-01-17 6:00	23-01-19 6:45	2.03
17	23-01-17 6:00	23-01-21 6:45	4.03
18	23-01-19 6:45	23-01-21 6:45	2.00
19	23-01-19 6:45	23-01-21 6:45	2.00
20	23-01-19 6:45	23-01-23 5:30	3.95
21	23-01-19 6:45	23-01-23 5:30	3.95
22	23-01-19 6:45	23-01-25 12:40	6.25
23	23-01-21 6:45	23-01-25 12:40	4.25
24	23-01-21 6:45	23-01-23 5:30	1.95
25	23-01-21 6:45	23-01-23 5:30	1.95
26	23-01-23 5:30	23-01-27 7:14	4.07
27	23-01-23 5:30	23-01-24 8:30	1.13
28	23-01-23 5:30	23-01-25 12:40	2.30
29	23-01-23 5:30	23-01-25 12:40	2.30

https://doi.org/10.5194/egusphere-2026-4321
Preprint. Discussion started: 27 August 2026

30	23-01-24 8:30	23-01-27 7:14	2.95
31	23-01-25 12:40	23-01-27 7:14	1.77
32	23-01-25 12:40	23-01-29 7:10	3.77
33	23-01-25 12:40	23-01-31 6:54	5.76
34	23-01-25 12:40	23-02-02 7:00	7.76
35	23-01-27 7:14	23-01-29 7:10	2.00
36	23-01-27 7:14	23-01-29 7:10	2.00
37	23-01-27 7:14	23-01-31 6:54	3.99
38	23-01-27 7:14	23-02-02 7:00	5.99
39	23-01-27 7:14	23-02-04 7:00	7.99
40	23-01-29 7:10	23-01-31 6:54	1.99
41	23-01-29 7:10	23-02-02 7:00	3.99
42	23-01-29 7:10	23-02-04 7:00	5.99
43	23-02-02 7:00	23-02-04 7:00	2.00
44	23-02-02 7:00	23-02-04 7:00	2.00
45	23-02-02 7:00	23-02-04 7:00	2.00
46	23-01-31 6:54	23-02-04 7:00	4.00
47	23-01-31 6:54	23-02-04 7:00	4.00
48	23-01-25 12:40	23-02-04 7:00	9.76

750

https://doi.org/10.5194/egusphere-2026-4321
Preprint. Discussion started: 27 August 2026

Table B3. The list of marine samples.

MMP sample no.	Date and time of sampling	sampled volume, L	Sampling place	latitude	longitude	tide level
1	15-01-23 11:45	36	MCOH north	6°46'37.76"N	73°11'1.41"E	high tide
2	15-01-23 12:45	27	MCOH west	6°46'32.98"N	73°10'54.50"E	high tide
3	19-01-23 8:00	60	MCOH north	6°46'37.76"N	73°11'1.41"E	low tide
4	21-01-23 9:45	64	MCOH north	6°46'37.76"N	73°11'1.41"E	low tide
5	23-01-23 8:00	64	MCOH north	6°46'37.76"N	73°11'1.41"E	high tide
6	24-01-23 11:00	64	MCOH north	6°46'37.76"N	73°11'1.41"E	high tide
7	24-01-23 13:00	48	Undhoali Beach	6°46'5.89"N	73°10'29.89"E	high tide
8	26-01-23 3:26	80	Kelaa	6°56'19.56"N	73°12'19.92"E	low tide
9	26-01-23 7:14	48	Thuraakunu	7° 6'23.28"N	72°53'14.82"E	low tide
10	27-01-23 12:04	48	MCOH north	6°46'37.76"N	73°11'1.41"E	high tide
11	29-01-23 14:30	40	Gan	0°41'15.71"S	73° 9'4.25"E	high tide
12	31-01-23 14:00	44	Gan	0°40'58.92"S	73° 8'37.13"E	moderate
13	02-02-23 12:30	52	MCOH north	6°46'37.76"N	73°11'1.41"E	low tide
14	04-02-23 12:30	56	MCOH north	6°46'37.76"N	73°11'1.41"E	low tide
15	07-02-23 9:15	50	Hulhumalé	4°12'51.74"N	73°32'43.53"E	high tide

https://doi.org/10.5194/egusphere-2026-4321
Preprint. Discussion started: 27 August 2026

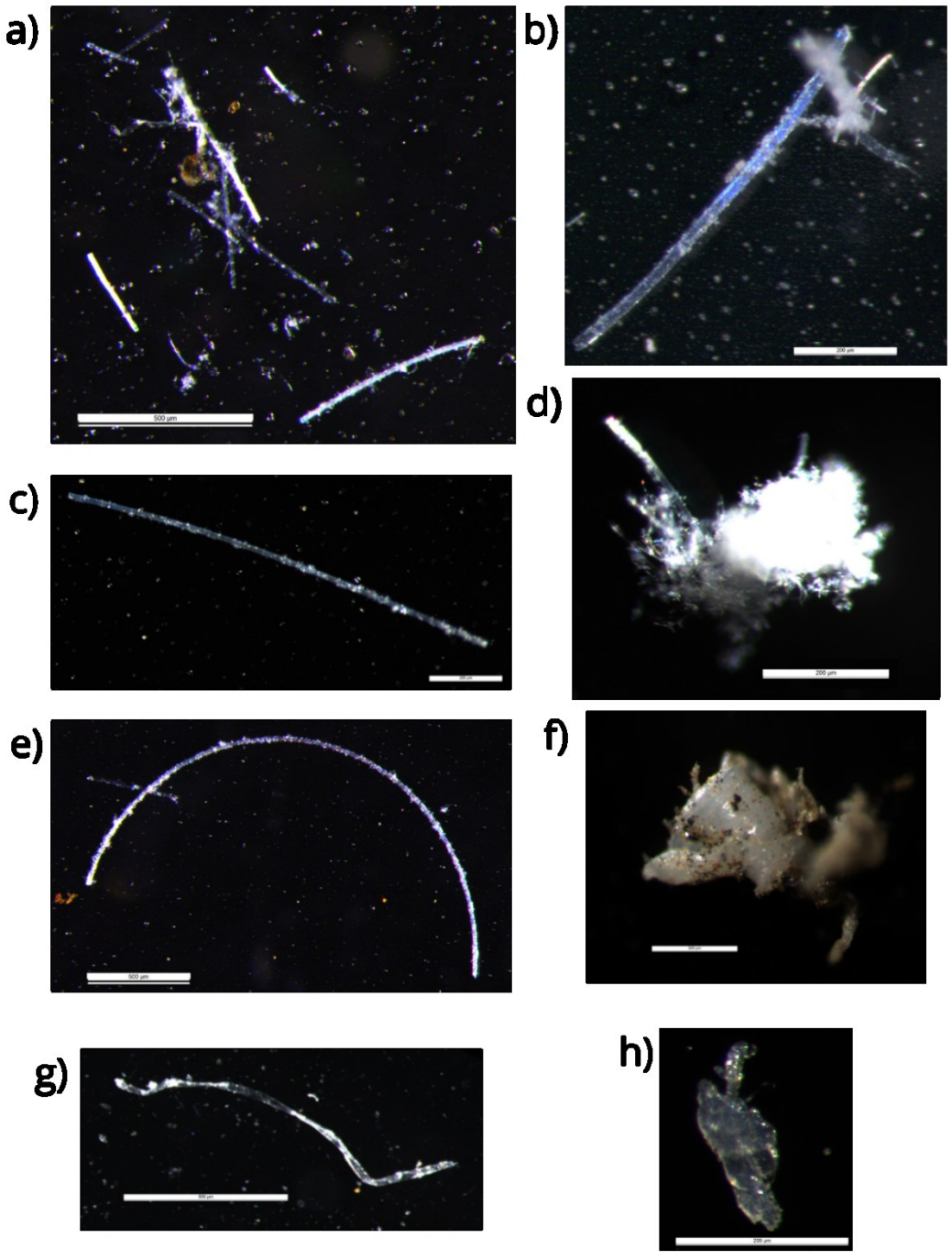

Figure B1. Representative airborne microparticles: (a) polyethylene (PE) fibres; (b) a polyethylene terephthalate (PET) fibre with an attached white PE fragment; (c) a PE fibre; (d) a PE fragment; (e) a PE fibre; (f) a polypropylene (PP) fragment; (g) a cellulose fibre; and (h) a PP film.

https://doi.org/10.5194/egusphere-2026-4321
Preprint. Discussion started: 27 August 2026

755

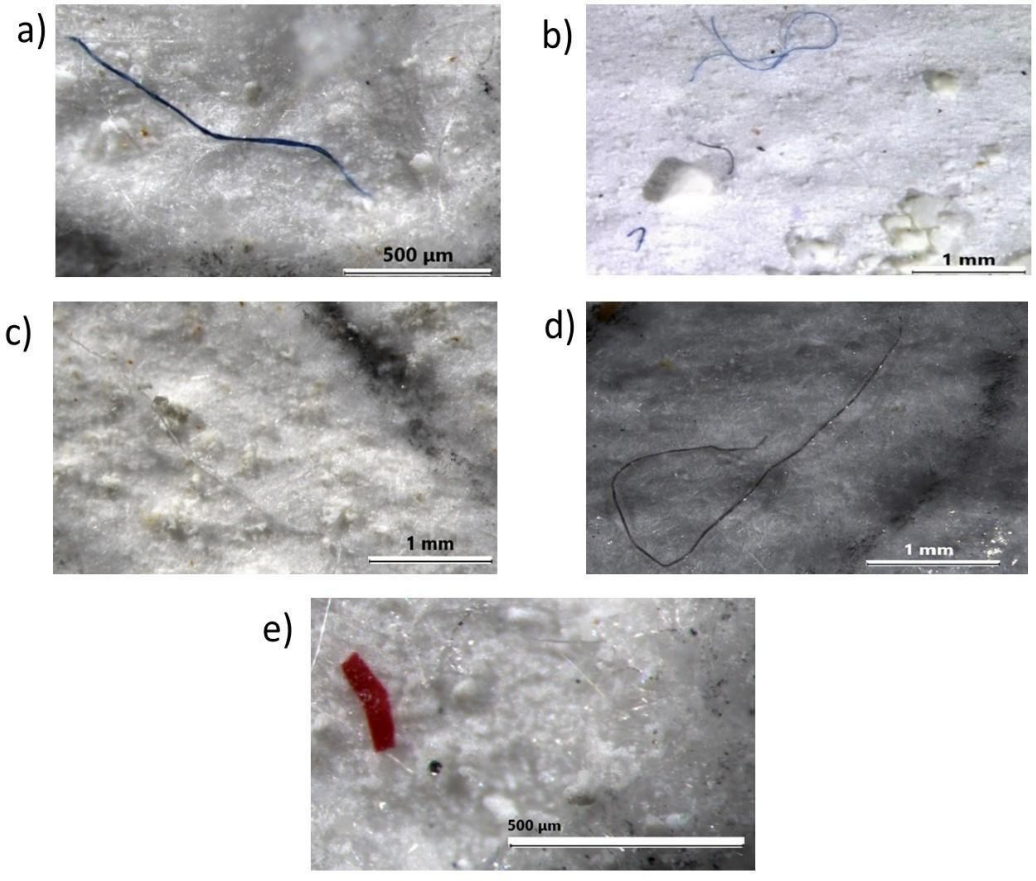

Figure B2. Representative airborne microparticles: (a, b) blue polyethylene terephthalate (PET) fibres; (c) a brown PET fibre; (d) a transparent polypropylene (PP) fibre; and (e) a pink paint-related fragment containing dye.

https://doi.org/10.5194/egusphere-2026-4321
Preprint. Discussion started: 27 August 2026

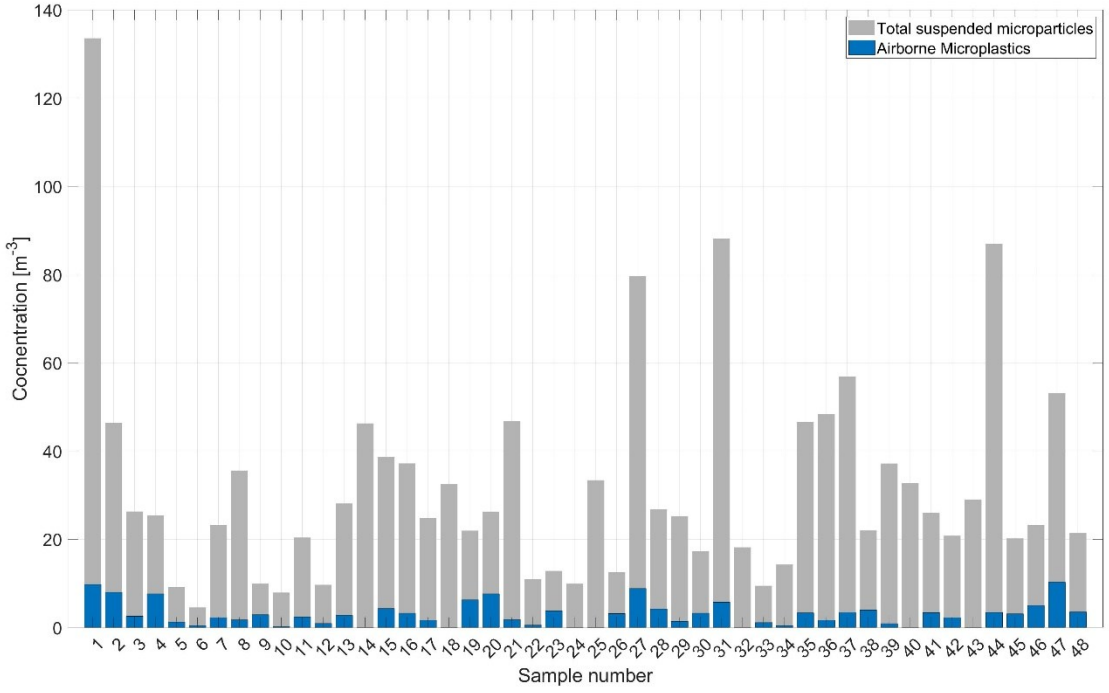

Figure B3. Number concentrations of total suspended microparticles (TSMP; grey bars) and airborne microplastics (AMP; blue bars) during the 48 deposition-box sampling periods at the Maldives Climate Observatory Hanimaadhoo (MCOH). 46 environmental samples and laboratory blanks 11 and 12; blanks were excluded from environmental statistics. TSMP comprises all detected microparticles, whereas AMP comprises the subset classified as microplastics using the optical-screening and spectroscopic-validation procedure described in Sects. 2.3 and 2.4. Consequently, the AMP concentration is included within, rather than additional to, the corresponding TSMP concentration. Note the logarithmic y axis.

https://doi.org/10.5194/egusphere-2026-4321
Preprint. Discussion started: 27 August 2026

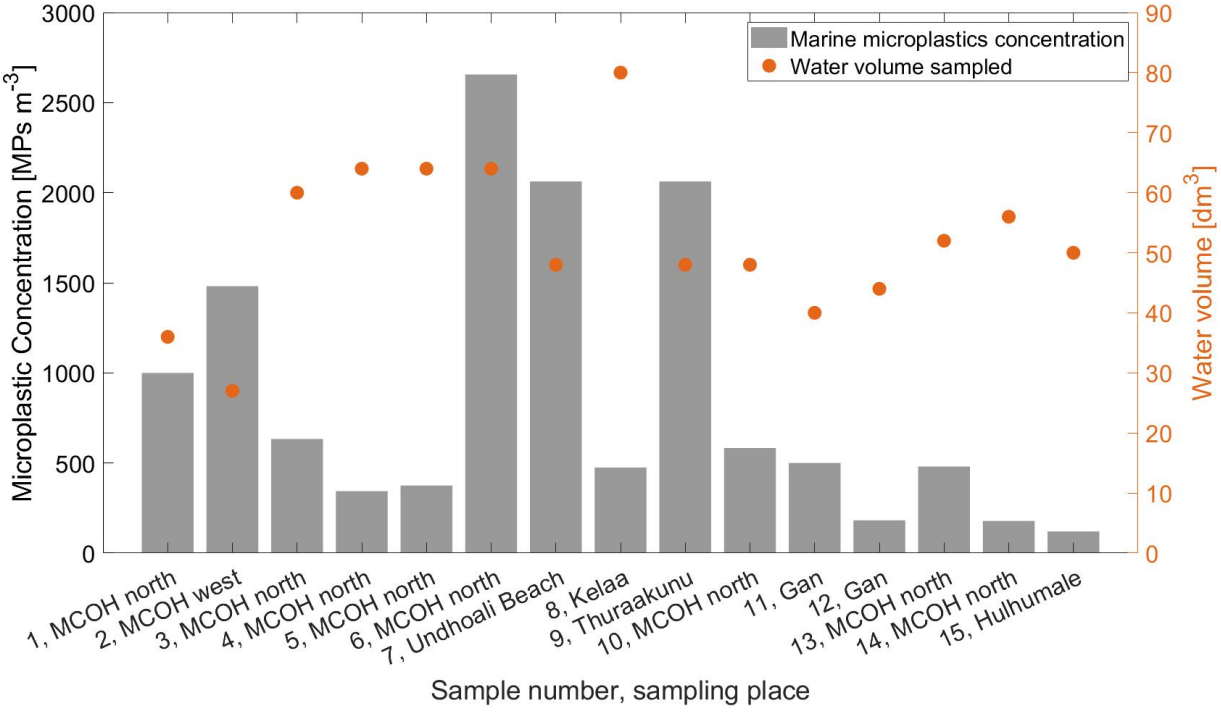

Figure B4. Concentrations of marine microplastics (MMP) were measured in seawater samples collected around the Maldives. Grey bars represent the microplastic concentration expressed as the number of particles per cubic metre (MP m^{-3}) for each sample (1–15). Orange circles indicate the volume of seawater filtered for each sample (dm^3), shown on the right vertical axis. Concentrations were calculated as the number of detected microplastic particles divided by the corresponding volume of filtered water. Variations in concentration partly reflect differences in local environmental conditions and sampling volume, including storm-driven resuspension and local coastal inputs.

Data availability.

Data referenced in this study can be accessed via the Zenodo: Markuszewski et al., (2026) https://doi.org/10.5281/zenodo.22102519

Author contributions

PiM, MM, LF, and DN conceptualised the study and designed the measurement campaign. PiM, SLH, and KB conducted the field measurements and sample collection. KS, MŚ, PJT, and AW performed the optical microscopy and µ-Raman analyses, including particle characterisation, polymer identification, and validation of the analytical results. LF, DN, MZ and ÖG supervised the research. KB provided access to the MCOH research infrastructure and coordinated local logistical support. PiM was responsible for project administration and funding acquisition. PiM curated and analysed the data, performed the

https://doi.org/10.5194/egusphere-2026-4321
Preprint. Discussion started: 27 August 2026

statistical analyses, prepared the visualisations, and wrote the original draft of the manuscript. MM, KS, MŚ, PJT, LF, KB, MZ, AW, PrzM, DN, ÖG, and SLH contributed to the interpretation of the results and reviewed and edited the manuscript.

Competing interests

The authors declare that they have no conflict of interest

Acknowledgements

The authors sincerely thank Prof. Sebastian Mahlik (Gdańsk University) for providing access to the Raman laboratory, where the Raman-based identification analyses presented in this study were carried out.

The authors acknowledge the support of Prof. Krzysztof Markowicz (Warsaw University), who advised us on the processing of aerosol properties data.

In addition, we thank the technical staff, Mr Sharafulla Thoha, Miss. Mariyam, and Mr Faruhaadh Moosa at MCOH, the Maldives Meteorological Service and the Government of the Republic of Maldives for their support during the field campaign.

This work is also an output of the GEMMA Centre in the framework of the project MUR TECLA "Dipartimenti di Eccellenza 2023–2027".

Grammarly and ChatGPT were used solely to improve grammar, sentence structure, and readability. All suggested changes were reviewed and approved by the authors, who retain full responsibility for the scientific content and final wording of the manuscript.

Figure 1b was produced with the Giovanni online data system, developed and maintained by the NASA GES DISC.

Financial support

This work was financially supported by the National Science Centre, Poland (Grant 2023/49/B/ST10/00513), the Swedish Research Council (VR, Grant 2021-05225), and the Bolin Centre (under Research Theme 1).

References

Acker, J. G., and Leptoukh, G.: Online analysis enhances use of NASA Earth science data, Eos, Transactions American Geophysical Union, 88, 14–17, https://doi.org/10.1029/2007EO020003, 2007.

Allen, D., Allen, S., Abbasi, S., Baker, A., Bergmann, M., Brahney, J., Butler, T., Duce, R. A., Eckhardt, S., Evangeliou, N., Jickells, T., Kanakidou, M., Kershaw, P., Laj, P., Levermore, J., Li, D., Liss, P., Liu, K., Mahowald, N., Masque, P., Materić, D., Mayes, A. G., McGinnity, P., Osvath, I., Prather, K. A., Prospero, J. M., Revell, L. E., Sander, S. G., Shim, W.

https://doi.org/10.5194/egusphere-2026-4321
Preprint. Discussion started: 27 August 2026

J., Slade, J., Stein, A., Tarasova, O., and Wright, S.: Microplastics and nanoplastics in the marine-atmosphere environment, Nature Reviews Earth & Environment, 3, 393–405, https://doi.org/10.1038/s43017-022-00292-x, 2022.

Allen, S., Allen, D., Moss, K., Le Roux, G., Phoenix, V. R., and Sonke, J. E.: Examination of the ocean as a source for atmospheric microplastics, PLOS ONE, 15, e0232746, https://doi.org/10.1371/journal.pone.0232746, 2020.

Allen, S., Allen, D., Phoenix, V. R., Le Roux, G., Durántez Jiménez, P., Simonneau, A., Binet, S., and Galop, D.: Atmospheric transport and deposition of microplastics in a remote mountain catchment, Nature Geoscience, 12, 339–344, https://doi.org/10.1038/s41561-019-0335-5, 2019.

Andreae, M. O., and Rosenfeld, D.: Aerosol–cloud–precipitation interactions. Part 1. The nature and sources of cloud-active aerosols, Earth-Science Reviews, 89, 13–41, https://doi.org/10.1016/j.earscirev.2008.03.001, 2008.

Arthur, C., Baker, J., and Bamford, H. (Eds.): Proceedings of the International Research Workshop on the Occurrence, Effects, and Fate of Microplastic Marine Debris, 9–11 September 2008, University of Washington Tacoma, Tacoma, WA, USA, NOAA Technical Memorandum NOS-OR&R-30, National Oceanic and Atmospheric Administration, Silver Spring, MD, USA, 2009.

Athapaththu, A. M. A. I. K., Thushari, G. G. N., Dias, P. C. B., Abeygunawardena, A. P., Egodauyana, K. P. U. T., Liyanage, N. P. P., Pitawala, H. M. J. C., and Senevirathna, J. D. M.: Plastics in surface water of southern coastal belt of Sri Lanka (Northern Indian Ocean): Distribution and characterization by FTIR, Marine Pollution Bulletin, 161, 111750, https://doi.org/10.1016/j.marpolbul.2020.111750, 2020.

Auta, H. S., Emenike, C., and Fauziah, S.: Distribution and importance of microplastics in the marine environment: A review of the sources, fate, effects, and potential solutions, Environment International, 102, 165–176, https://doi.org/10.1016/j.envint.2017.02.013, 2017.

Bond, T. C., Doherty, S. J., Fahey, D. W., Forster, P. M., Berntsen, T., DeAngelo, B. J., Flanner, M. G., Ghan, S., Kärcher, B., Koch, D., Kinne, S., Kondo, Y., Quinn, P. K., Sarofim, M. C., Schultz, M. G., Schulz, M., Venkataraman, C., Zhang, H., Zhang, S., Bellouin, N., Guttikunda, S. K., Hopke, P. K., Jacobson, M. Z., Kaiser, J. W., Klimont, Z., Lohmann, U., Schwarz, J. P., Shindell, D., Storelvmo, T., Warren, S. G., and Zender, C. S.: Bounding the role of black carbon in the climate system: A scientific assessment, Journal of Geophysical Research: Atmospheres, 118, 5380–5552, https://doi.org/10.1002/jgrd.50171, 2013.

Boucher, J., and Friot, D.: Primary microplastics in the oceans: a global evaluation of sources, International Union for Conservation of Nature, Gland, Switzerland, 43 pp., https://doi.org/10.2305/IUCN.CH.2017.01.en, 2017.

Brahney, J., Mahowald, N., Prank, M., Cornwell, G., Klimont, Z., Matsui, H., and Prather, K. A.: Constraining the atmospheric limb of the plastic cycle, Proceedings of the National Academy of Sciences, 118, e2020719118, https://doi.org/10.1073/pnas.2020719118, 2021.

Budhavant, K., Andersson, A., Bosch, C., Kruså, M., Murthaza, A., Zahid, and Gustafsson, Ö.: Apportioned contributions of PM2.5 fine aerosol particles over the Maldives (northern Indian Ocean) from local sources vs long-range transport, Science of the Total Environment, 536, 72–78, https://doi.org/10.1016/j.scitotenv.2015.07.059, 2015.

https://doi.org/10.5194/egusphere-2026-4321
Preprint. Discussion started: 27 August 2026

Budhavant, K., Andersson, A., Holmstrand, H., Bikkina, P., Bikkina, S., Satheesh, S. K., and Gustafsson, Ö.: Enhanced Light-Absorption of Black Carbon in Rainwater Compared With Aerosols Over the Northern Indian Ocean, Journal of Geophysical Research: Atmospheres, 125, e2019JD031246, https://doi.org/10.1029/2019JD031246, 2020.

Budhavant, K., Andersson, A., Holmstrand, H., Satheesh, S. K., and Gustafsson, Ö.: Black carbon aerosols over Indian Ocean have unique source fingerprint and optical characteristics during monsoon season, Proceedings of the National Academy of Sciences, 120, e2210005120, https://doi.org/10.1073/pnas.2210005120, 2023.

Budhavant, K., Bikkina, S., Andersson, A., Asmi, E., Backman, J., Kesti, J., Zahid, H., Satheesh, S. K., and Gustafsson, Ö.: Anthropogenic fine aerosols dominate the wintertime regime over the northern Indian Ocean, Tellus B: Chemical and Physical Meteorology, 70, 1464871, https://doi.org/10.1080/16000889.2018.1464871, 2018.

Budhavant, K., Manoj, M. R., Nair, H. R. C. R., Gaita, S. M., Holmstrand, H., Salam, A., Muslim, A., Satheesh, S. K., and Gustafsson, Ö.: Changing optical properties of black carbon and brown carbon aerosols during long-range transport from the Indo-Gangetic Plain to the equatorial Indian Ocean, Atmospheric Chemistry and Physics, 24, 11911–11925, https://doi.org/10.5194/acp-24-11911-2024, 2024.

Chen, Q., Shi, G., Revell, L. E., Zhang, J., Zuo, C., Wang, D., Le Ru, E. C., Wu, G., and Mitrano, D. M.: Long-range atmospheric transport of microplastics across the southern hemisphere, Nature Communications, 14, 7898, https://doi.org/10.1038/s41467-023-43695-0, 2023.

Clarke, S., Holmstrand, H., Budhavant, K., Remani, M., Haslett, S., Rodiouchkina, K., Kooijman, E., and Gustafsson, Ö.: Isotopic apportionment of sulfate aerosols between natural and anthropogenic sources in the outflow of South Asia, Atmospheric Chemistry and Physics, 26, 5333–5343, https://doi.org/10.5194/acp-26-5333-2026, 2026.

Connan, M., Perold, V., Dilley, B. J., Barbraud, C., Cherel, Y., and Ryan, P. G.: The Indian Ocean 'garbage patch': Empirical evidence from floating macro-litter, Marine Pollution Bulletin, 169, 112559, https://doi.org/10.1016/j.marpolbul.2021.112559, 2021.

Corrigan, C. E., Ramanathan, V., and Schauer, J. J.: Impact of monsoon transitions on the physical and optical properties of aerosols, Journal of Geophysical Research: Atmospheres, 111, D18208, https://doi.org/10.1029/2005JD006370, 2006.

Dasari, S., Andersson, A., Kim, S.-W., Holmstrand, H., Budhavant, K., and Gustafsson, Ö.: Observationally Constrained Wintertime Emission Fluxes and Atmospheric Lifetime of Black Carbon in South Asia, Environmental Science & Technology Letters, 12, 710–717, https://doi.org/10.1021/acs.estlett.5c00079, 2025.

Donaldson, K., and Tran, C. L.: Inflammation caused by particles and fibres, Inhalation Toxicology, 14, 5–27, https://doi.org/10.1080/089583701753338613, 2002.

Dris, R., Gasperi, J., Mirande, C., Mandin, C., Guerrouache, M., Langlois, V., and Tassin, B.: A first overview of textile fibers, including microplastics, in indoor and outdoor environments, Environmental Pollution, 221, 453–458, https://doi.org/10.1016/j.envpol.2016.12.013, 2017.

https://doi.org/10.5194/egusphere-2026-4321
Preprint. Discussion started: 27 August 2026

Eberhard, T., Casillas, G., Zarus, G. M., and Barr, D. B.: Systematic review of microplastics and nanoplastics in indoor and outdoor air: identifying a framework and data needs for quantifying human inhalation exposures, Journal of Exposure Science & Environmental Epidemiology, 34, 185–196, https://doi.org/10.1038/s41370-023-00634-x, 2024.

Enyoh, C. E., Verla, A. W., Verla, E. N., Ibe, F. C., and Amaobi, C. E.: Airborne microplastics: a review study on method for analysis, occurrence, movement and risks, Environmental Monitoring and Assessment, 191, 668, https://doi.org/10.1007/s10661-019-7842-0, 2019.

European Commission: Commission Recommendation of 18 October 2011 on the definition of nanomaterial (2011/696/EU), Official Journal of the European Union, L 275, 38–40, 2011.

Ferrero, L., Casati, M., Nobili, L., D'Angelo, L., Rovelli, G., Sangiorgi, G., Rizzi, C., Perrone, M. G., Sansonetti, A., Conti, C., Bolzacchini, E., Bernardi, E., and Vassura, I.: Chemically and size-resolved particulate matter dry deposition on stone and surrogate surfaces inside and outside the low emission zone of Milan: application of a newly developed "Deposition Box", Environmental Science and Pollution Research, 25, 9402–9415, https://doi.org/10.1007/s11356-018-1220-2, 2018.

Ferrero, L., Losi, N., Rigler, M., Gregorič, A., Colombi, C., D'Angelo, L., Cuccia, E., Cefalì, A. M., Gini, I., Doldi, A., Cerri, S., Maroni, P., Cipriano, D., Markuszewski, P., and Bolzacchini, E.: Determining the Aethalometer multiple scattering enhancement factor C from the filter loading parameter, Science of the Total Environment, 917, 170221, https://doi.org/10.1016/j.scitotenv.2024.170221, 2024.

Ferrero, L., Scibetta, L., Markuszewski, P., Mazurkiewicz, M., Drozdowska, V., Makuch, P., Jutrzenka-Trzebiatowska, P., Zaleska-Medynska, A., Andò, S., Saliu, F., Nilsson, E. D., and Bolzacchini, E.: Airborne and marine microplastics from an oceanographic survey at the Baltic Sea: An emerging role of air-sea interaction?, Science of the Total Environment, 824, 153709, https://doi.org/10.1016/j.scitotenv.2022.153709, 2022.

Ghosh, A., Mandal, A., Karmakar, J., Mazumdar, S., and Darbha, G. K.: A pilot investigation of PM10-bound atmospheric microplastics over a protected mangrove ecosystem: Role of land–sea breeze circulation in marine and terrestrial inputs, Science of the Total Environment, 1004, 180797, https://doi.org/10.1016/j.scitotenv.2025.180797, 2025.

GMAO, Global Modeling and Assimilation Office and Pawson, S.: MERRA-2 tavg1_2d_aer_Nx: 2d, 1-hourly, time-averaged, single-level, assimilation, aerosol diagnostics, version 5.12.4 [data set], NASA Goddard Earth Sciences Data and Information Services Center, https://doi.org/10.5067/KLICLTZ8EM9D, 2015 (data accessed: 5 June 2026).

González-Pleiter, M., Edo, C., Aguilera, Á., Viúdez-Moreiras, D., Pulido-Reyes, G., González-Toril, E., Osuna, S., de Diego-Castilla, G., Leganés, F., Fernández-Piñas, F., and Rosal, R.: Occurrence and transport of microplastics sampled within and above the planetary boundary layer, Science of the Total Environment, 761, 143213, https://doi.org/10.1016/j.scitotenv.2020.143213, 2021.

Gustafsson, Ö., Budhavant, K., Chimurkar, N., Clarke, S., Dreyfus, G., Gong, X., Klimont, Z., Klingmüller, K., Kim, S.-W., Lelieveld, J., Myhre, G., Nair, H. R. C. R., Peng, J., Ramanathan, V., Rana, A., Manoj, M. R., Satheesh, S. K., Venkataraman, C., and Zhang, Q.: Atmospheric black carbon in the climate system, Nature Reviews Earth & Environment, 7, 312–328, https://doi.org/10.1038/s43017-026-00773-3, 2026.

https://doi.org/10.5194/egusphere-2026-4321
Preprint. Discussion started: 27 August 2026

Gustafsson, Ö., Kruså, M., Zencak, Z., Sheesley, R. J., Granat, L., Engström, E., Praveen, P. S., Rao, P. S. P., Leck, C., and Rodhe, H.: Brown Clouds over South Asia: Biomass or Fossil Fuel Combustion?, Science, 323, 495–498, https://doi.org/10.1126/science.1164857, 2009.

Hildebrandt, L., El Gareb, F., Zimmermann, T., Klein, O., Kerstan, A., Emeis, K.-C., and Pröfrock, D.: Spatial distribution of microplastics in the tropical Indian Ocean based on laser direct infrared imaging and microwave-assisted matrix digestion, Environmental Pollution, 307, 119547, https://doi.org/10.1016/j.envpol.2022.119547, 2022.

Imhof, H. K., Sigl, R., Brauer, E., Feyl, S., Giesemann, P., Klink, S., Leupolz, K., Löder, M. G. J., Löschel, L. A., Missun, J., Muszynski, S., Ramsperger, A. F. R. M., Schrank, I., Speck, S., Steibl, S., Trotter, B., Winter, I., and Laforsch, C.: Spatial and temporal variation of macro-, meso- and microplastic abundance on a remote coral island of the Maldives, Indian Ocean, Marine Pollution Bulletin, 116, 340–347, https://doi.org/10.1016/j.marpolbul.2017.01.010, 2017.

Isa, V., Saliu, F., Becchi, A., Spadaccino, G., Quinto, M., Veronelli, M., Lasagni, M., Galli, P., and Lavorano, S.: Impacts of microplastics on reef-building corals: Disentangling the contribution of the chain scission products released by weathering, Science of the Total Environment, 975, 179239, https://doi.org/10.1016/j.scitotenv.2025.179239, 2025.

Islam, M. R., Welker, J., Salam, A., and Stone, E. A.: Plastic Burning Impacts on Atmospheric Fine Particulate Matter at Urban and Rural Sites in the USA and Bangladesh, ACS Environmental Au, 2, 409–417, https://doi.org/10.1021/acsenvironau.1c00054, 2022.

Kannankai, M. P., and Devipriya, S. P.: Atmospheric microplastic deposition in a coastal city of India: The influence of a landfill source on monsoon winds, Science of the Total Environment, 908, 168235, https://doi.org/10.1016/j.scitotenv.2023.168235, 2024.

Kapmeier, F., and Gonçalves, P.: Wasted paradise? Policies for Small Island States to manage tourism-driven growth while controlling waste generation: the case of the Maldives, System Dynamics Review, 34, 172–221, https://doi.org/10.1002/sdr.1607, 2018.

Kaushik, A., Gupta, P., Kumar, A., Saha, M., Varghese, E., Shukla, G., Suresh, K., and Gunthe, S. S.: Identification and physico-chemical characterization of microplastics in marine aerosols over the northeast Arabian Sea, Science of the Total Environment, 912, 168705, https://doi.org/10.1016/j.scitotenv.2023.168705, 2024.

Kaza, S., Yao, L., Bhada-Tata, P., and Van Woerden, F.: What a waste 2.0: a global snapshot of solid waste management to 2050, World Bank, Washington, DC, https://doi.org/10.1596/978-1-4648-1329-0, 2018.

Kováts, N., Hubai, K., Sainnokhoi, T.-A., Eck-Varanka, B., Hoffer, A., Tóth, Á., Kakasi, B., and Teke, G.: Ecotoxic emissions generated by illegal burning of household waste, Chemosphere, 298, 134263, https://doi.org/10.1016/j.chemosphere.2022.134263, 2022.

Kum, G., Berglund, O., and Hollander, J.: Lost in definition: unravelling microplastics from marine coatings through bibliometrics science mapping in thematic analysis and systematic narrative literature review, Environmental Sciences Europe, 37, 38, https://doi.org/10.1186/s12302-025-01070-4, 2025.

https://doi.org/10.5194/egusphere-2026-4321
Preprint. Discussion started: 27 August 2026

Lewis, E. R., and Schwartz, S. E.: Sea salt aerosol production: mechanisms, methods, measurements, and models – a critical review, Geophysical Monograph Series, 152, American Geophysical Union, Washington, DC, https://doi.org/10.1029/GM152, 2004.

Li, J., Gao, F., Zhang, D., Cao, W., and Zhao, C.: Zonal Distribution Characteristics of Microplastics in the Southern Indian Ocean and the Influence of Ocean Current, Journal of Marine Science and Engineering, 10, 290, https://doi.org/10.3390/jmse10020290, 2022.

Markuszewski, P., Budhavant, K., Gustafsson, Ö., Jutrzenka-Trzebiatowska, P., Stawiarz, K., Śmiszek, M., Nilsson, E. D., and Haslett, S.: Airborne and marine microplastics and atmospheric context measurements at the Maldives Climate Observatory Hanimaadhoo and adjacent coastal waters, January–February 2023, Zenodo [data set], https://doi.org/10.5281/zenodo.22102519, 2026.

Müller, T., Henzing, J. S., de Leeuw, G., Wiedensohler, A., Alastuey, A., Angelov, H., Bizjak, M., Collaud Coen, M., Engström, J. E., Gruening, C., Hillamo, R., Hoffer, A., Imre, K., Ivanow, P., Jennings, G., Sun, J. Y., Kalivitis, N., Karlsson, H., Komppula, M., Laj, P., Li, S.-M., Lunder, C., Marinoni, A., Martins dos Santos, S., Moerman, M., Nowak, A., Ogren, J. A., Petzold, A., Pichon, J. M., Rodriquez, S., Sharma, S., Sheridan, P. J., Teinilä, K., Tuch, T., Viana, M., Virkkula, A., Weingartner, E., Wilhelm, R., and Wang, Y. Q.: Characterization and intercomparison of aerosol absorption photometers: result of two intercomparison workshops, Atmospheric Measurement Techniques, 4, 245–268, https://doi.org/10.5194/amt-4-245-2011, 2011.

Müller, T., Virkkula, A., and Ogren, J. A.: Constrained two-stream algorithm for calculating aerosol light absorption coefficient from the Particle Soot Absorption Photometer, Atmospheric Measurement Techniques, 7, 4049–4070, https://doi.org/10.5194/amt-7-4049-2014, 2014.

Munshi, S., Banerjee, S., and Chakraborty, I.: Thilafushi a toxic bomb: learning from an island's solid-waste-management practice, International Journal of Architecture and Infrastructure Planning, 8, 1–12, 2022.

Nair, H. R. C. R., Budhavant, K., Manoj, M. R., Andersson, A., Satheesh, S. K., Ramanathan, V., and Gustafsson, Ö.: Aerosol demasking enhances climate warming over South Asia, npj Climate and Atmospheric Science, 6, 39, https://doi.org/10.1038/s41612-023-00367-6, 2023.

O'Dowd, C. D., and de Leeuw, G.: Marine aerosol production: a review of the current knowledge, Philosophical Transactions of the Royal Society A: Mathematical, Physical and Engineering Sciences, 365, 1753–1774, https://doi.org/10.1098/rsta.2007.2043, 2007.

Oehlschlägel, L. M., Schmid, S., Lehmann, M., Gekle, S., and Held, A.: Water–air transfer rates of microplastic particles through bubble bursting as a function of particle size, Microplastics and Nanoplastics, 4, 1, https://doi.org/10.1186/s43591-023-00079-x, 2024.

Patti, T. B., Fobert, E. K., Reeves, S. E., and Burke da Silva, K.: Spatial distribution of microplastics around an inhabited coral island in the Maldives, Indian Ocean, Science of the Total Environment, 748, 141263, https://doi.org/10.1016/j.scitotenv.2020.141263, 2020.

https://doi.org/10.5194/egusphere-2026-4321
Preprint. Discussion started: 27 August 2026

Pattiaratchi, C., van der Mheen, M., Schlundt, C., Narayanaswamy, B. E., Sura, A., Hajbane, S., White, R., Kumar, N., Fernandes, M., and Wijeratne, S.: Plastics in the Indian Ocean – sources, transport, distribution, and impacts, Ocean Science, 18, 1–28, https://doi.org/10.5194/os-18-1-2022, 2022.

Perera, K., Ziajahromi, S., Bengtson Nash, S., Manage, P. M., and Leusch, F. D. L.: Airborne Microplastics in Indoor and Outdoor Environments of a Developing Country in South Asia: Abundance, Distribution, Morphology, and Possible Sources, Environmental Science & Technology, 56, 16676–16685, https://doi.org/10.1021/acs.est.2c05885, 2022.

Perraki, M., Skliros, V., Mecaj, P., Vasileiou, E., Salmas, C., Papanikolaou, I., and Stamatis, G.: Identification of Microplastics Using μ-Raman Spectroscopy in Surface and Groundwater Bodies of SE Attica, Greece, Water, 16, 843, https://doi.org/10.3390/w16060843, 2024.

Petzold, A., Ogren, J. A., Fiebig, M., Laj, P., Li, S.-M., Baltensperger, U., Holzer-Popp, T., Kinne, S., Pappalardo, G., Sugimoto, N., Wehrli, C., Wiedensohler, A., and Zhang, X.-Y.: Recommendations for reporting "black carbon" measurements, Atmospheric Chemistry and Physics, 13, 8365–8379, https://doi.org/10.5194/acp-13-8365-2013, 2013.

Prata, J. C., Castro, J. L., da Costa, J. P., Duarte, A. C., Rocha-Santos, T., and Cerqueira, M.: The importance of contamination control in airborne fibers and microplastic sampling: Experiences from indoor and outdoor air sampling in Aveiro, Portugal, Marine Pollution Bulletin, 159, 111522, https://doi.org/10.1016/j.marpolbul.2020.111522, 2020.

Prata, J. C., Padrão, J., Khan, M. T., and Walker, T. R.: Do's and don'ts of microplastic research: a comprehensive guide, Water Emerging Contaminants & Nanoplastics, 3, 8, https://doi.org/10.20517/wecn.2023.61, 2024.

Raguso, C., Saliu, F., Lasagni, M., Galli, P., Clemenza, M., and Montano, S.: First detection of microplastics in reef-building corals from a Maldivian atoll, Marine Pollution Bulletin, 180, 113773, https://doi.org/10.1016/j.marpolbul.2022.113773, 2022.

Ramachandran, S., and Rupakheti, M.: Inter-annual and seasonal variations in columnar aerosol characteristics and radiative effects over the Pokhara Valley in the Himalayan foothills – Composition, radiative forcing, and atmospheric heating, Environmental Pollution, 264, 114799, https://doi.org/10.1016/j.envpol.2020.114799, 2020.

Ramana, M. V., and Ramanathan, V.: Abrupt transition from natural to anthropogenic aerosol radiative forcing: Observations at the ABC-Maldives Climate Observatory, Journal of Geophysical Research: Atmospheres, 111, D20207, https://doi.org/10.1029/2006JD007063, 2006.

Ramanathan, V., and Carmichael, G.: Global and regional climate changes due to black carbon, Nature Geoscience, 1, 221–227, https://doi.org/10.1038/ngeo156, 2008.

Ramanathan, V., Crutzen, P. J., Lelieveld, J., Mitra, A. P., Althausen, D., Anderson, J., Andreae, M. O., Cantrell, W., Cass, G. R., Chung, C. E., Clarke, A. D., Coakley, J. A., Collins, W. D., Conant, W. C., Dulac, F., Heintzenberg, J., Heymsfield, A. J., Holben, B., Howell, S., Hudson, J., Jayaraman, A., Kiehl, J. T., Krishnamurti, T. N., Lubin, D., McFarquhar, G., Novakov, T., Ogren, J. A., Podgorny, I. A., Prather, K., Priestley, K., Prospero, J. M., Quinn, P. K., Rajeev, K., Rasch, P., Rupert, S., Sadourny, R., Satheesh, S. K., Shaw, G. E., Sheridan, P., and Valero, F. P. J.: Indian Ocean Experiment: An

https://doi.org/10.5194/egusphere-2026-4321
Preprint. Discussion started: 27 August 2026

integrated analysis of the climate forcing and effects of the great Indo-Asian haze, Journal of Geophysical Research: Atmospheres, 106, 28371–28398, https://doi.org/10.1029/2001JD900133, 2001.

Rao, M. N., Ghude, S. D., Nivdange, S. D., Panchang, R., Pipal, A. S., Mukherjee, A., Sharma, H., and Kumar, V.: Characterization and health risk assessment of airborne microplastics in Delhi NCR, Scientific Reports, 15, 25662, https://doi.org/10.1038/s41598-025-04306-8, 2025.

Rifa, T., and Hossain, M. B.: Micro Plastic Pollution in South Asia: The Impact of Plastic Pollution over the Unsustainable Development Goals, Lex Publica, 9, 1–28, https://doi.org/10.58829/lp.9.2.2022.01-28, 2022.

Rochman, C. M., Manzano, C., Hentschel, B. T., Simonich, S. L. M., and Hoh, E.: Polystyrene Plastic: A Source and Sink for Polycyclic Aromatic Hydrocarbons in the Marine Environment, Environmental Science & Technology, 47, 13976–13984, https://doi.org/10.1021/es403605f, 2013.

Royle, J., Jack, B., Parris, H., Elliott, T., Castillo, A. C., Kalawana, S., Nashfa, H., and Woodall, L. C.: Plastic Drawdown: A rapid assessment tool for developing national responses to plastic pollution when data availability is limited, as demonstrated in the Maldives, Global Environmental Change, 72, 102442, https://doi.org/10.1016/j.gloenvcha.2021.102442, 2022.

Saliu, F., Montano, S., Garavaglia, M. G., Lasagni, M., Seveso, D., and Galli, P.: Microplastic and charred microplastic in the Faafu Atoll, Maldives, Marine Pollution Bulletin, 136, 464–471, https://doi.org/10.1016/j.marpolbul.2018.09.023, 2018.

Saliu, F., Montano, S., Leoni, B., Lasagni, M., and Galli, P.: Microplastics as a threat to coral reef environments: Detection of phthalate esters in neuston and scleractinian corals from the Faafu Atoll, Maldives, Mar. Pollut. Bull., 142, 234–241, https://doi.org/10.1016/j.marpolbul.2019.03.043, 2019.

Schlitzer, R.: Ocean Data View, https://odv.awi.de (last access: 24 July 2026), 2025.

Sheesley, R. J., Kirillova, E., Andersson, A., Kruså, M., Praveen, P. S., Budhavant, K., Safai, P. D., Rao, P. S. P., and Gustafsson, Ö.: Year-round radiocarbon-based source apportionment of carbonaceous aerosols at two background sites in South Asia, Journal of Geophysical Research: Atmospheres, 117, D10202, https://doi.org/10.1029/2011JD017161, 2012.

Spencer, M. T., Holecek, J. C., Corrigan, C. E., Ramanathan, V., and Prather, K. A.: Size-resolved chemical composition of aerosol particles during a monsoonal transition period over the Indian Ocean, Journal of Geophysical Research: Atmospheres, 113, D16305, https://doi.org/10.1029/2007JD008657, 2008.

Stegelius, K., Thompson, P., Karbiener, P., Markuszewski, P., Prevot, A. S. H., Tripathi, S. N., Mohr, C., Heikkinen, L., Budhavant, K., and Haslett, S. L.: Aerosol processing during long-range transport governs the chemical composition of haze over the northern Indian Ocean, EGUsphere [preprint], https://doi.org/10.5194/egusphere-2026-914, 2026.

Stevens, G. M. W., and Froman, N.: The Maldives Archipelago, in: World Seas: an Environmental Evaluation, 2nd edn., edited by: Sheppard, C., Academic Press, 211–236, https://doi.org/10.1016/B978-0-08-100853-9.00010-5, 2019.

Tauhiduzzaman, M., Salsabil, N., Khatun, K., Muhaiminul Haque, M., Habib, A., Shamima Akter, M., Islam, S., Hasibuzzaman, M., Rahman, I. M., Ahmmed, M., Zaman, S., Chakraborty, T. K., and Ghosh, G. C.: Atmospheric microplastics deposition in Dhaka City, Bangladesh: occurrence, distribution and ecological risk assessment, Atmospheric Pollution Research, 17, 102856, https://doi.org/10.1016/j.apr.2025.102856, 2025.

https://doi.org/10.5194/egusphere-2026-4321
Preprint. Discussion started: 27 August 2026

Trainic, M., Flores, J. M., Pinkas, I., Pedrotti, M. L., Lombard, F., Bourdin, G., Gorsky, G., Boss, E., Rudich, Y., Vardi, A., and Koren, I.: Airborne microplastic particles detected in the remote marine atmosphere, Communications Earth & Environment, 1, 64, https://doi.org/10.1038/s43247-020-00061-y, 2020.

Turner, A.: Paint particles in the marine environment: An overlooked component of microplastics, Water Research X, 12, 100110, https://doi.org/10.1016/j.wroa.2021.100110, 2021.

van der Does, M., Knippertz, P., Zschenderlein, P., Harrison, R. G., and Stuut, J.-B. W.: The mysterious long-range transport of giant mineral dust particles, Science Advances, 4, eaau2768, https://doi.org/10.1126/sciadv.aau2768, 2018.

Vasse, G. F., and Melgert, B. N.: Microplastic and plastic pollution: impact on respiratory disease and health, European Respiratory Review, 33, 230226, https://doi.org/10.1183/16000617.0226-2023, 2024.

Wang, X., Li, C., Liu, K., Zhu, L., Song, Z., and Li, D.: Atmospheric microplastic over the South China Sea and East Indian Ocean: abundance, distribution and source, Journal of Hazardous Materials, 389, 121846, https://doi.org/10.1016/j.jhazmat.2019.121846, 2020.

Wang, Z., Hu, M., Fan, J., Zheng, H., Wang, C., Ahmad, M., Li, L., Zhao, G., Zhang, G., Zhang, Y., Hu, J., and Wang, Y.: Microplastic pollution in the Indian Ocean: Fiber-dominated contamination and comparative bioaccumulation in Auxis thazard and Symplectoteuthis oualaniensis, Marine Environmental Research, 210, 107304, https://doi.org/10.1016/j.marenvres.2025.107304, 2025.

Zeng, E. Y. (Ed.): Microplastic contamination in aquatic environments: an emerging matter of environmental urgency, Elsevier, Amsterdam, the Netherlands, 2023.

Zhang, W., Zhang, S., Zhao, Q., Qu, L., Ma, D., and Wang, J.: Spatio-temporal distribution of plastic and microplastic debris in the surface water of the Bohai Sea, China, Marine Pollution Bulletin, 158, 111343, https://doi.org/10.1016/j.marpolbul.2020.111343, 2020.

Zhou, L., Li, J., Zhao, C., Yin, J., Ding, J., Cao, W., and Fan, W.: Overview of monitoring methods and environmental distribution: Microplastics in the Indian Ocean, Marine Pollution Bulletin, 214, 117715, https://doi.org/10.1016/j.marpolbul.2025.117715, 2025.